

STRUCTURAL CHANGES IN STRETCHED COLLAGEN FIBRILS AS A FUNCTION OF RELAXATION TIMES

by

S M Asif Iqbal

Submitted in partial fulfilment of the requirements
for the degree of Master of Science

at

Dalhousie University
Halifax, Nova Scotia
September 2018

© Copyright by S M Asif Iqbal, 2018

Dedicated to my father.

Table of Contents

List of Tables	vi
List of Figures	vii
Abstract	xi
List of Abbreviations Used	xii
Acknowledgements	xiii
Chapter 1 Introduction	1
1.1 Collagen Fibrils and Structural Hierarchy in tendons.....	1
1.2 Tendon mechanics	3
1.3 Mechanical Properties of Single Collagen Fibrils	6
1.4 Molecular Denaturation Detection with CHP	9
1.5 Overview of experimental techniques used in investigating viscoelastic properties and rupture mechanics in single fibril level.	11
1.6 Research Questions.....	16
Chapter 2 Materials and Methods	17
2.1 CDET collection, collagen fibril extraction and sample preparation.....	17
2.2 Pulling fine tipped glass rods for gluing purpose	18
2.3 Isolation of collagen fibril segments and gluing procedure	18

2.4 AFM cantilever characterization and spring constant calibration	20
2.5 Pre-manipulated fibril imaging	21
2.6 AFM basic operation, experimental set-up and relaxation method.....	21
2.7 Overview of relations between mechanical parameters	23
2.8 Post-manipulated Fibril imaging	26
2.9 Sample preparation for post-manipulated fluorescence imaging and fluorescence imaging protocol	26
2.10 Data Analysis	27
2.10.1 Fibril height profiling	27
2.10.2 Fibril cross section profiling	28
2.10.3 Fluorescence Intensity Profiling	29
2.10.4 D-Band Measurement	30
2.10.5 Statistical Analysis	31
Chapter 3 Results.....	32
3.1 Collagen fibrils morphology and supramolecular structure before and after manipulation	33
3.2 Tensile loading and release lead to molecular denaturation	38
3.3 Fluorescence intensity profile for different strain levels	39
3.4 Fluorescence Intensity and Strain dependence	42

3.5 Relation between observed fluorescence intensity and fibril cross-sectional area loss due to manipulation	46
3.6 Quantitative measurement of molecular denaturation due to manipulation	49
3.7 Energetics involved in molecular denaturation process	53
Chapter 4 Discussion	55
4.1 Fibril Damage.....	55
4.2 Calibration of Molecular unfolding	57
4.3 The energetics of mechanical denaturation	58
4.4 Comparison with Rupture Mechanics.....	61
4.5 Physiological Significance	63
Chapter 5 Conclusion	65
References	67
Appendix.....	79

List of Tables

Table 3.1: Collagen fibrils morphology before manipulation (measured value \pm SD) for each relaxation time.....	34
Table 3.2: The morphological change in fibril after relaxation (measured value \pm SD), for each relaxation time.....	36
Table 3.3: Summary of D-band measurements for each relaxation time.....	37
Table 3.4: Detailed presentation of fitting parameters of the cases shown in Fig. 3.12 (A-F, respectively), the number of unfolded molecules represent weighted average value of all these slopes and corresponding standard deviation is weighted mean of the error.....	51

List of Figures

Fig.1.1: The hierarchical structure of tendon	1
Fig.1.2: Stress-strain response from rat tail tendon	4
Fig 1.3: The power-temperature curve in DSC response for extensor and flexor tendons	6
Fig.1.4: Stress-Strain response of positional and energy storing tendon single fibril and corresponding Post rupture morphology of positional fibrils	8
Fig.1.5: Average of stress–strain curves for different strain groups, fluorescence images of the samples that experienced 5, 10.5 and 15% strain, and the brightfield image for the 15% strained fascicle	10
Fig.1.6: Stepwise detailed schematic drawing showing the gluing procedure and tensile testing of single fibril with vertical force microscopy by Yang et al	12
Fig.1.7: Schematic of tensile testing experiment on a single fibril performed by AFM vertical force spectroscopy by shen et al	13
Fig.1.8: Diagram showing different parts of a MEMS device for tensile testing experiment_	15
Fig.1.9: Stress vs. time plot that showed viscoelastic response of collagen fibrils	16
Fig.2.1: Fibril isolation and gluing by Quigley et al	19
Fig.2.2: Bruker Tap525A AFM probe viewed under SEM	20
Fig.2.3: A simple illustration of the bowstring geometry and basic AFM operation_	23

Fig.2.4: Bowstring geometry of fibril pulling	24
Fig.2.5: Transformation of voltage-distance curve to Force-time and Force-distance curve_	25
Fig.2.6: Pulling sequence, the fibril was pulled by the AFM tip (17% strain)	26
Fig.2.7: Height profiling and Area profiling of fibril before and after manipulation_	28
Fig.2.8: Example of height-distance profile at each location where cross section of the fibril was measured	29
Fig.2.9: Fibril height profile and FFT for D-band measurement.....	30
Fig.3.1: Optical microscopy frames taken before manipulation, at the maximum strain and after release for the three different relaxation times_	33
Fig.3.2: Height and Cross-Sectional area profile of the control profile	35
Fig.3.3: The mean D-band spacing before and after manipulation for all 14 fibrils and distribution of D-band difference	37
Fig.3.4: Mean fluorescence intensity along the fibrils for the control case and the three different relaxation times	39
Fig.3.5: An example of fluorescence intensity profile and corresponding fluorescence image where the fibril experienced two different strains	40
Fig.3.6: Mean fluorescence intensity between the low strain and high strain region of all the fibrils that experienced asymmetric stretching_	41

Fig.3.7: Plot of strain difference and fluorescence difference for asymmetric cases.....42

Fig.3.8: Relationship between fluorescence intensity and the strain applied on each fibril for the three different relaxation times, strain categories introduced_..... 44

Fig.3.9: Relation between coefficient of variation of fluorescence and coefficient of variation of area before manipulation 45

Fig.3.10: Pre-manipulated fibril cross-section and corresponding fluorescence intensity at every micron length 45

Fig.3.11: Computer simulated “ball and stick” model of collagen triple-helix and denatured state induced by heat 47

Fig.3.12: Relationship has been shown between mean area loss and fluorescence intensity for two different cases 48

Fig.3.13: Cases where statistically significant relationship has been found between mean area difference and fluorescence intensity 49

Fig.3.14: Three strain groups in terms of number of molecules lost due to manipulation based on the calibrated number from the slope 52

Fig.3.15: Plot of change in volume vs. weighted average of strain 53

Fig.3.16: Fraction of volume loss after manipulation as function of mechanical energy and the mechanical energy has been plotted against weighted strain average_ 54

Fig.4.1: Sigmoidal fitting of mean fluorescence intensity and strain plot for all fibrils and different relaxation time categories 56

Fig.4.2: Two probable loading mechanisms of molecular unfolding and related results 60

Fig.4.3: Non linear response of the collagen molecular denaturation as a function of strain..... 63

Abstract

The collagen fibrils are the main building block of connective tissues in mammals where they fulfill both structural and mechanical roles. The structure of a fibril is based on collagen molecules that self-assemble into micro-fibrils and sub-fibrils stabilized by hydrogen bonds and covalent crosslinks. The non-integer staggering of collagen molecules results in a characteristic D-band pattern along the fibril with a periodicity of 67nm. Fibrils were extracted from bovine extensor tendons, around 40 microns long segments were isolated (n=14) and glued, imaged with AFM before manipulation and then stretched between 5% and 20% strain, held at that strain for 150 seconds (n=8), 1 second (n=3), or 1500 seconds (n=3) then released. The manipulated fibrils were then imaged using AFM to characterize morphological changes. To assess whether stress relaxation led to denaturation (uncoiling) of collagen molecules, fluorescent collagen hybridizing peptide (CHP, a probe specific to denatured collagen) was applied to the samples and binding was measured using a Zeiss LSM 710 upright confocal microscope. We observed that stretching followed by stress relaxation did not break the fibrils and did not change significantly the value of the D-band. However, our fluorescence microscopy results indicate that some collagen molecules unfold within the fibril due to the stretching and relaxation protocol. AFM mapping of the fibrils cross section indicates a correlation between molecular denaturation as measured through fluorescence and loss of cross-sectional area. In addition, the mechanical energy density for denaturing a full single fibril was estimated. To our knowledge, this is the first demonstration of molecular denaturation within a single collagen fibril during a non-disruptive tensile test.

List of Abbreviations Used

TEM	transmission electron microscopy
AFM	atomic force microscopy
PG	proteoglycans
GAG	glycosaminoglycans
SDFT	superficial digital flexor tendon
CDET	common digital extensor tendon
DSC	differential scanning calorimetry
HIT	hydrothermal isometric tension
SEM	scanning electron microscopy
CHP	collagen hybridizing peptide
MMP	matrix metalloproteinase
CF-CHP	carboxyfluorescein labeled collagen hybridizing peptide
MEMS	microelectromechanical systems
MDET	medial digital extensor tendon
LDET	lateral digital extensor tendon
QNM	quantitative nanomechanical mapping
DIC	differential interference contrast
ROI	region of interest
VMD	visual molecular dynamics

Acknowledgements

It's my honest realization that this work has been possible for direct and close supervision of Laurent Kreplak. My committee members Sam Veres and Andrew Rutenberg have been very supportive and helped to direct the project in the right direction. As a MSc candidate, I'd say that they are perfect mentors for training a graduate student. I'd also like to thank my friends Ajan Ramachandran, Matthew, Dylan, Chris Peacock, and Arjya Sarkar and Soumoshree Sarkar for listening my thoughts on this project many times which is helpful for any kind of ongoing research.

Chapter 1

Introduction

1.1 Collagen Fibrils and Structural Hierarchy in tendons

Collagen is the most abundant protein in tendons, bones, cornea, skin and other connective tissues. At least 25-28 different collagen types have been identified genetically and among them collagen I is the most abundant in the human body¹⁻³. Collagen I forms fibrils that are recognized as the main load-bearing component in connective tissues, especially in tendon and ligament^{4,5}, and that are often compared to mechanical ropes⁶. The structural hierarchy of collagen based tissues all the way to the molecular level is well established, and is thought to be responsible for many of their unique mechanical properties⁷. In tendon, this hierarchy can be well visualized with the aid of Fig.1.1.

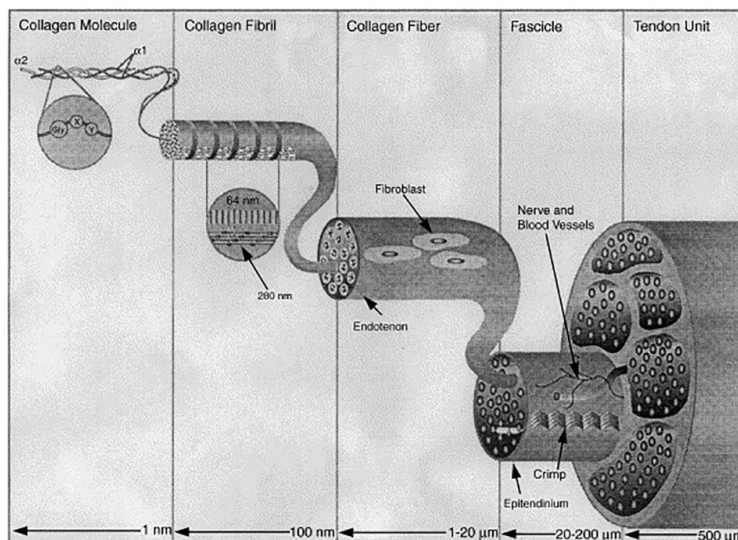


Fig.1.1: The hierarchical structure of tendon, tendon level is seven order greater than the smallest unit, collagen molecule. Figure adapted from⁷

The smallest structural unit of tendons is the collagen molecule which is a triple helix^{8,9}, where three left handed polypeptide chains (referred to as alpha chains) coil around each other in such a fashion that the molecule is ultimately right handed, type I collagen molecules contain two $\alpha 1$ chains and one $\alpha 2$ chain. The generalized amino acid sequence of collagen molecule is (Gly -X-Y)_n where X and Y can be any amino acid^{10,11} (mostly Proline and hydroxy-Proline) and n can be 337-343 which varies by collagen type. Glycine remains at the core of the triple helix as it is small enough⁹, provides tight packing¹² while other two amino acids are exposed⁸. The short non-helical ends are known as telopeptides, situated at N- and C-termini, and are essential for fibril formation. The collagen molecule (also referred to as tropocollagen) is around 300 nm in length, has a diameter around 1.5 nm and a molecular weight of 285 kDa¹³.

The next level of hierarchy is the fibril level, Type I collagen fibril length within tendon is estimated to be in the order of few millimeters¹⁴. The fundamental structural unit of a fibril is the microfibril, a bundle of five collagen molecules in cross-section that are longitudinally arranged in a quarter-staggered way to create a 'gap' and 'overlap' region of different molecular density. This quarter-stagger motif persists through the fibril's entire cross-section and gives rise to the characteristic 64-67 nm D-Band pattern^{15,16}, clearly visible in transmission electron microscopy (TEM)¹⁷ or atomic force microscopy (AFM)^{18,19}. Furthermore, *in vivo*, collagen molecules are cross linked together within fibrils by covalent bonds in order to achieve stability and the biologically required fibril's tensile strength²⁰⁻²³. The fibrils are then further organized into fibril bundles and fascicles through a multi-step process¹⁴.

Macroscopically, the basic constituents of tendons are collagen and water, collagen contributes 70-85% of tendon dry mass, while water contributes 50-65% of wet mass²⁴⁻²⁷. Among the collagenous material, the most abundant is collagen type I with collagen type III and V present in small amounts²⁸⁻³². Among non-collagenous materials, proteoglycans (PGs, 0.5-3% of dry mass) and elastin fibers (<2%) are thought to be significant³³⁻³⁵. PGs are glycoproteins, attached to carbohydrate moieties, glycosaminoglycans (GAGs) by covalent bonds, that bind water and can be found at the surface of the fibril, however, we still do not have a definitive technique that can confirm whether they are actually located inside or outside of the fibril³⁶⁻³⁸. PGs also create a gel-like structure with other glycoproteins that helps collagen fibrils to remain attached³⁹ and are considered to be tissue organizers⁴⁰.

1.2 Tendon mechanics

There have been a number of investigations on tendon mechanics using single tendon models, for example rat tail tendon^{35,41-43}, bovine tail tendon^{25,44} etc. Fig. 1.2 illustrates the stress strain behavior of a typical rat tail tendon⁴⁵. The curve can be divided in three distinct regions, different features are observed in each region. The low strain or toe region corresponds to less than 3% strain that have been identified in polarized light microscopy where the macroscopic crimp of collagen fibres, in the order of 100 microns, is removed⁴⁶. In next level (the heel region), the fibrils start to be recruited in tension and the lateral arrangement of collagen molecules inside the fibril gets more organized as a result of the straightening of molecular kinks happening within the gap regions and therefore entropy decreases⁴⁵. In the linear region, the collagen molecules get

stretched and/or start sliding as the cross-links get engaged in tension⁴⁷. The last two regions are not visible in light microscopy, therefore (synchrotron) X-ray scattering has been used as the investigation tool. Overall, due to the complex structural hierarchy, the fibril level strain as assessed by measurement of D-band spacing always lags behind the tendon-applied strain. Therefore, separate investigation of the fibril level under tension is important to understand tendon mechanics.

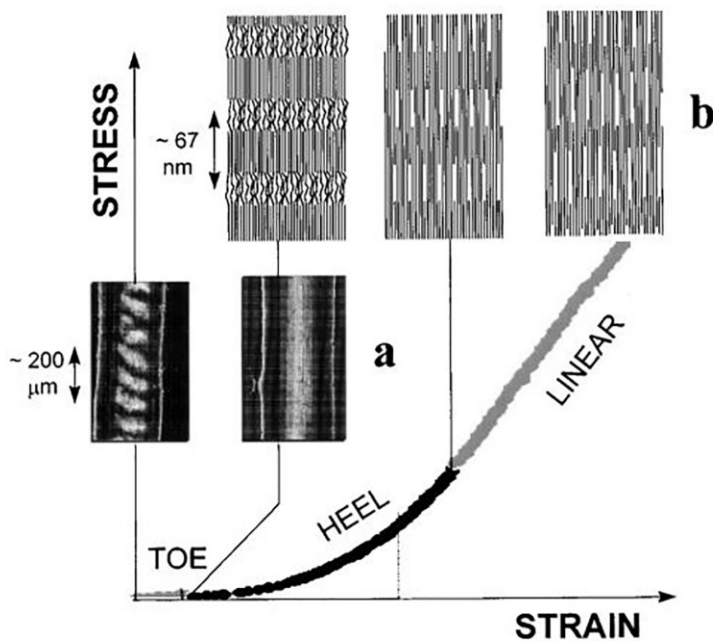


Fig.1.2: Stress-strain response from rat tail tendon, macroscopic crimp in the toe region is removed⁴⁶(a). The structural changes in heel and linear region happen at the fibrillar level (b) which can not be observed in light microscopy. (Figure adapted from⁴⁵)

From the functional point of view, two different classes of tendon are often distinguished, energy storing and positional tendons^{48,49}. It has been revealed using the equine and bovine models that

these energy storing and positional tendons have distinct structure and mechanics. The superficial digital flexor tendon (SDFT) and common digital extensor tendon (CDET) pair of the equine and bovine forelimb have been studied extensively as energy storing tendon and positional tendon models, respectively^{24,50-52}. As the name indicates, the energy storing tendons are proposed to store and release energy to drive locomotion, they can sustain large stresses (69-75 MPa)⁵³. On the other side of the forelimb, the positional tendons maintain the hoof in position with respect to the forelimb and are exposed to smaller stress (8-36 MPa)⁵³.

How structural differences between SDFT and CDET leads to different mechanical properties, has been explored extensively by investigating SDFT and CDET extracted from equine and bovine forelimbs^{51,54}. Screen et al. investigated the extension and recovery of fascicles extracted from equine SDFT and CDET, SDFT fascicles seem to have an helical macrostructure which enables efficient recoil and less hysteresis loss⁵¹. Herod et al. also studied undamaged, ruptured and cyclically loaded SDFT and CDET extracted from bovine forelimbs⁵⁴. Differences in molecular structure was assessed using differential scanning calorimetry (DSC), hydrothermal isometric tension (HIT) and scanning electron microscopy (SEM). The DSC results indicated that collagen molecular packing is tighter in the SDFT compared to the CDET (Fig.1.3). The DSC analysis also showed that the denaturation energy is 58 ± 13.7 J/g for CDET and 40.7 ± 10.1 J/g for SDFT, based on dry sample weight. The HIT analysis indicated two results, the cross-links in SDFT are more heat stable and cross- link density was also comparatively higher in SDFT. Interestingly, the CDETs were found to be stronger and tougher than the SDFTs. SEM images of ruptured tendons showed

that CDETs experience discrete plastic damage, featured by repeated kinks, while SDFTs did not show such plastic deformation at the strain rate of 10%/s.

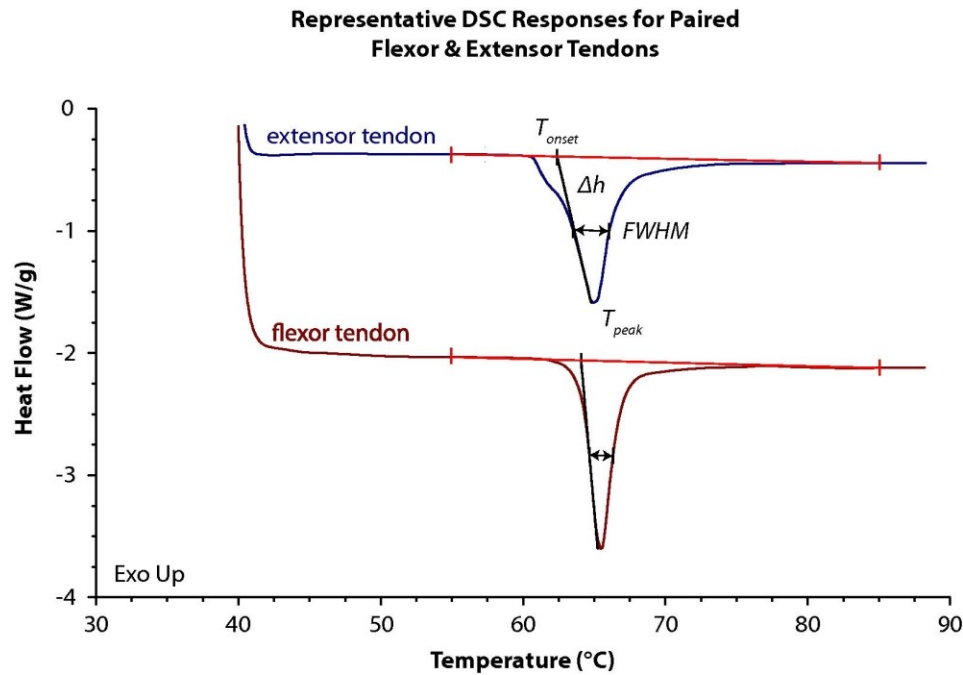


Fig 1.3: The power-temperature curve in DSC response for extensor (CDET) and flexor (SDFT) tendons, the flexor showed higher peak temperature and smaller full-width-half-maximum than the extensor. This indicates that flexor tendons are thermally more stable (Figure adapted from⁵⁴), which implies that they probably have tighter molecular packing.

1.3 Mechanical Properties of Single Collagen Fibrils

It is evident that the longitudinal collagen fibrils work as load bearing component of tendon which transmits force from bone to muscle^{4,5,35}. How the hierarchical structure of tendon, with PGs and other collagen-associated proteins contribute to overall mechanical properties, is an important

question in tissue biomechanics. From a structure-function point of view, it is expected that fibrils from different tissues should have structurally different characteristics, which enable tissues to perform different functions, and leads to different mechanical response. Quigley et al.⁵⁵ showed that single fibrils extracted from SDFT and CDET of bovine forelimbs have different mechanical response due to their difference in intermolecular crosslinking, the SDFT fibrils showed high strain stiffening and resistance to disruption compared to CDET fibrils. The mechanical response of single fibrils extracted from SDF and CDE is shown in Fig.1.4(A&B). The tensile tests were carried out using bowstring geometry⁵⁶, as a technical feature of this pulling technique, the stress-strain curve can only be measured for strains above typically 5%. This, however, does not affect the experimental findings and perspectives. It is clear from Fig.1.4(A&B) that fibrils extracted from positional and energy storing tendon respond differently to tension, the positional fibrils show a two phase behavior (Fig.1.4 A) while the energy storing fibrils show a three-phase behavior (Fig.1.4B). Below 10% strain, in both cases, the linear region corresponds to straightening of collagen triple helices. Around 10% strain, the fibrils from positional tendon start yielding, the molecules slide with respect to each other longitudinally until rupture. For the energy storing fibrils, despite showing a similar behavior at around 10% strain, these fibrils get stiffer around 15% strain and stiffening is sustained until failure. Svensson et al.⁵⁷ also reported similar behavior of fibrils extracted from human patellar tendon and rat tail tendon, the response of human patellar tendon fibrils were similar to bovine energy storing tendon fibrils while rat tail tendon fibrils behaved like bovine positional tendon fibrils. The post rupture structural features of positional collagen fibrils and energy storing fibrils are shown in Fig. 1.4(C&D) and clearly demonstrate two different failure mechanisms. The positional fibrils undergo plastic

deformation, serial kinks and shell delamination are common features, the fibril structure was disrupted significantly. The energy storing fibrils did not show such post-rupture features, the native D-band pattern even remained conserved up to the rupture site indicating that the supramolecular structure remained intact, shell delamination was not observed and kinks were rare and sparsely distributed along the fibril length.

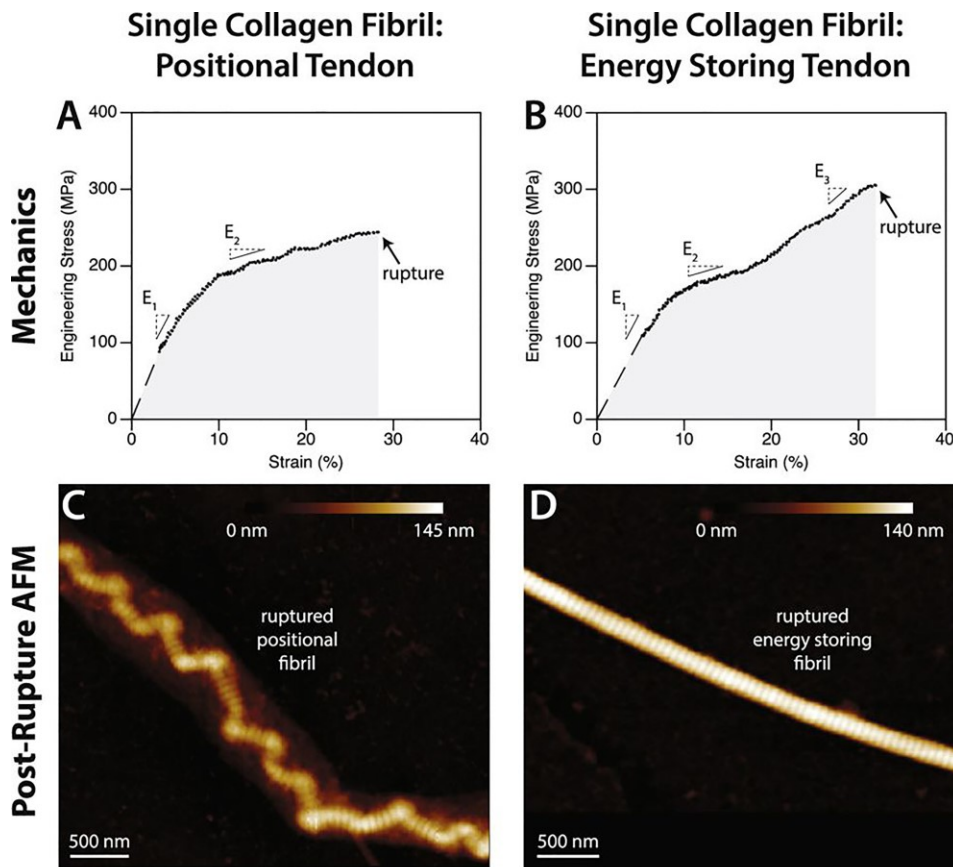


Fig.1.4: (A&B) Typical stress-Strain response of positional and energy storing tendon single fibril and corresponding post rupture morphology (C&D). (Figure adapted from⁵⁵)

1.4 Molecular Denaturation Detection with CHP

Collagen molecules can get denatured by heating or mechanical manipulation, there are several pathways of collagen molecular unfolding^{58–63}. Miles et al.⁶⁴ proposed that the denaturation process is an irreversible rate process that starts at thermally labile regions lacking hydroxyproline, near the C-terminal of the molecule and subsequently unzips the triple helix. Miles et al. also showed in another article that the thermally labile regions correspond to the gap region of the collagen ultrastructure²². As a consequence of denaturation, conformational changes happen in collagen molecules. The intermolecular cross-links break down, the triple helix unzipped and water molecules that stabilize the molecule are released, as a result, the molecule loses its native state^{64,65}. In case of mechanical loading, it was demonstrated that intermolecular sliding between the molecules and cross-linking between them are crucial factors for denaturation^{58,66}.

Molecular level damage was detected along collagen fibrils from cyclically overloaded, or ruptured tendons^{67–69}. In these studies, trypsin digestion susceptibility in ruptured or overloaded tendon was used as an indicator of molecular denaturation. Collagen hybridizing peptide (CHP) or collagen mimetic peptide is one of useful tools in molecular level damage detection⁷⁰. CHP is a synthetic peptide, it has glycine(G)–proline(P)–hydroxyproline(O) amino acid sequence that mimics the structural motif of natural collagen molecule and can successfully hybridize with denatured collagen denatured by heat or by matrix metalloproteinase (MMP) digestion both in vitro and in vivo^{70,71}. It has been clearly demonstrated that CHP, due to its neutral and hydrophilic sequence, has negligible binding affinity to intact collagen molecule or tissue^{70,72}. Zitnay et al.

recently used carboxyfluorescein (CF) labeled CHP (CF-CHP) to detect and quantitatively compare the molecular level damage where rat tail tendon fascicles that were mechanically stretched using a custom micro-mechanical test system up to a certain strain to cause subfailure level damage⁷³. Comparison between Fig.1.5 (a & c) showed that significant fluorescence intensity is observed when the stress-strain curve starts to move towards the plateau region (between 7.5-9% strain), an indication of permanent tissue damage. At 12-15% strain, the fluorescence intensity reaches at plateau (Fig.1.5c) which is correlated to the end of the stress plateau in stress-strain curves of Fig.1.5(a) where failure is observed. The fluorescence scans of 5, 10.5 and 15% strain samples clearly showed that CF-CHP staining increases with strain. The strained fascicles were also subjected for trypsin digestion for verification, the trypsin digestion increased in similar fashion as observed in case of fluorescence intensity and significant trypsin digestion was observed after 9% strain. All these results indicate that unfolding of collagen molecules occurs as soon as the tendon starts yielding.

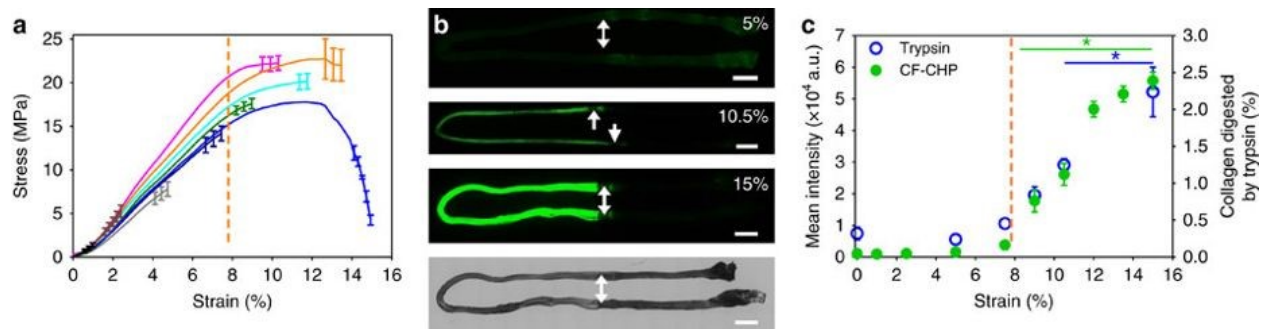


Fig.1.5:(a) Average of stress–strain curves for different strain groups (n=3) (b) fluorescence images of the samples that experienced 5, 10.5 and 15% strain, and the brightfield image for the 15% strained fascicle, increase in fluorescence intensity was observed with increased strain. And

(c) Fluorescence intensity and trypsin digestion vs. strain plot, threshold strain is indicated by the orange dotted line. (Fig. adapted from⁷³)

1.5 Overview of experimental techniques used in investigating viscoelastic properties and rupture mechanics at the single fibril level.

AFM vertical force spectroscopy has been used by several groups for observing stress-strain behavior, stress relaxation and viscoelastic behavior and rupture mechanics in single fibril level^{57,74–77}. Yang et al. performed vertical force spectroscopy for tensile testing of native and cross-linked collagen⁷⁷. The experimental set up of this work has been presented in (Fig.1.6). A two-component epoxy was used to glue the two end of a selected fibril crossing the glass-teflon interface using a triangular AFM cantilever, later with the aid of a rectangular cantilever, the fibril was stretched from one end. The non-sticking property of Teflon allows the rectangular cantilever to stretch the fibril while the glass surface keeps the other end of the fibril attached to the substrate. The study was designed to observe the influence of cross-linking on native collagen fibril by means of stress relaxation testing which also demonstrated the viscoelastic nature of collagen fibrils. They found two relaxation times – a fast component of 1.8 s and a slow component of 63 s for native collagen fibrils by fitting the stress-time curve with a Maxwell model. Addition of Glutaraldehyde and EDC/NHS zero-length cross-linker increased longer relaxation times (to 216 s and 252 s, respectively) which implies that sliding between the molecules is hindered because of cross-linkers. However, Glutaraldehyde was also able to increase the shorter relaxation times (from 1.8 s to 3.7 s) which supported the existence of microfibrils since it generates cross-links not only between the molecules but also between

microfibrils. Graham et al. used very similar technique to study vitro-assembled human type I collagen fibrils⁷⁸. However, unlike the method used by Yang et al. they did not use epoxy or glue droplet for AFM tip-fibril attachment or fibril-substrate attachment, relied on surface adhesion property of collagen fibrils. The force-elongation curve obtained in stretching was consistent with the worm-like chain (WLC) model⁷⁸.

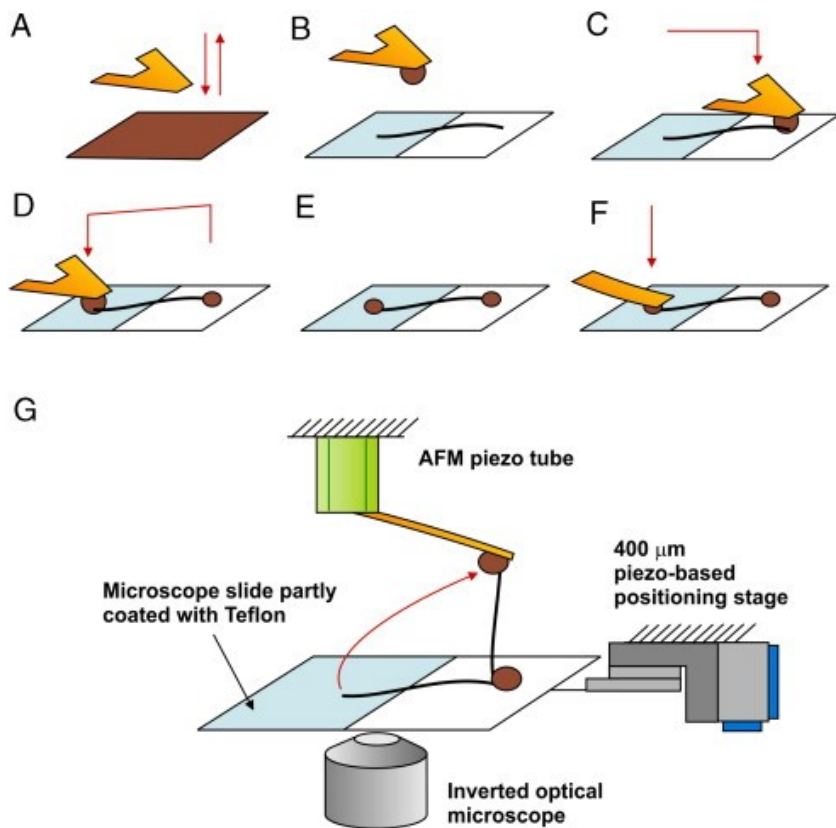


Fig. 1.6:(A-G) Stepwise detailed schematic drawing showing the gluing procedure and tensile testing of single fibril with vertical force microscopy. Figure adapted from⁷⁷

Svensson et al. also studied viscoelasticity and fracture mechanics of single collagen fibrils extracted from Human Patellar Tendon(HPT) and Rat Tail Tendon(RTT) using AFM vertical force spectroscopy in several studies.^{57,74,76} In these studies, similar method have been used for tensile testing where the experimental procedure was partly developed by van der Rijt et al⁷⁹. Fig. 1.7 summarizes the experimental procedure where two single collagen fibrils extracted from human fascicles were used for tensile testing using AFM approach. A single fibril was attached between AFM cantilever and substrate using epoxy glue, cyclic tensile test was performed at six different strain rates in the pre-yield region. In addition, stepwise relaxation testing was done to understand viscoelastic response. This was the first time demonstration of viscoelastic response at the single fibril level.

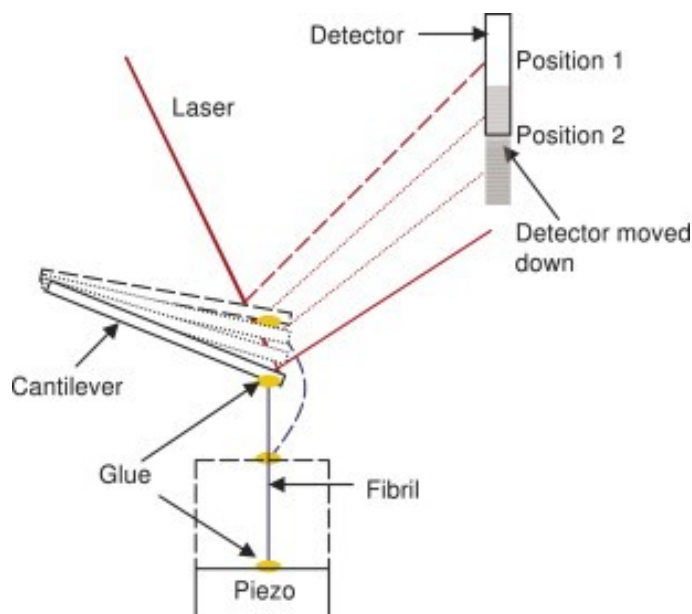


Fig. 1.7: Schematic of tensile testing experiment on a single fibril performed by AFM vertical force spectroscopy. Depending on the position of the piezo, the fibril gets relaxed or stretched. As a result, laser hits at different position of detector. Figure adapted from⁷⁴

MEMS (microelectromechanical systems) device has been used in several studies by Shen et al. to perform large-strain uniaxial tensile testing as well as combined creep and stress relaxation studies of single collagen fibrils⁸⁰⁻⁸². Fig.1.8 shows MEMS devices where the collagen fibril was suspended between the Fixed and Movable pads, mounted on a piezo stage of single axis-of-motion⁸². Uniaxial strain was applied by changing the relative distance between the fixed and movable pads controlled by the piezo stage. In this study Shen et al. conducted stress relaxation test of eight collagen fibrils extracted from sea cucumber. The stress relaxation behavior was fitted with the Maxwell Weichert models, indicating that fibrils show viscoelastic behavior (Fig.1.9). The variability observed in viscoelastic behavior was proposed to be a result of variability in cross-link density, fibril geometry and small sample number. They proposed that during stress relaxation the collagen molecules unwind and straighten first, then slide with respect to one another. Also, during relaxation the water molecules around the collagen molecules rearrange anywhere between 0.5 nm to 100 nm length-scale (radial collagen molecule spacing to fibril diameter)

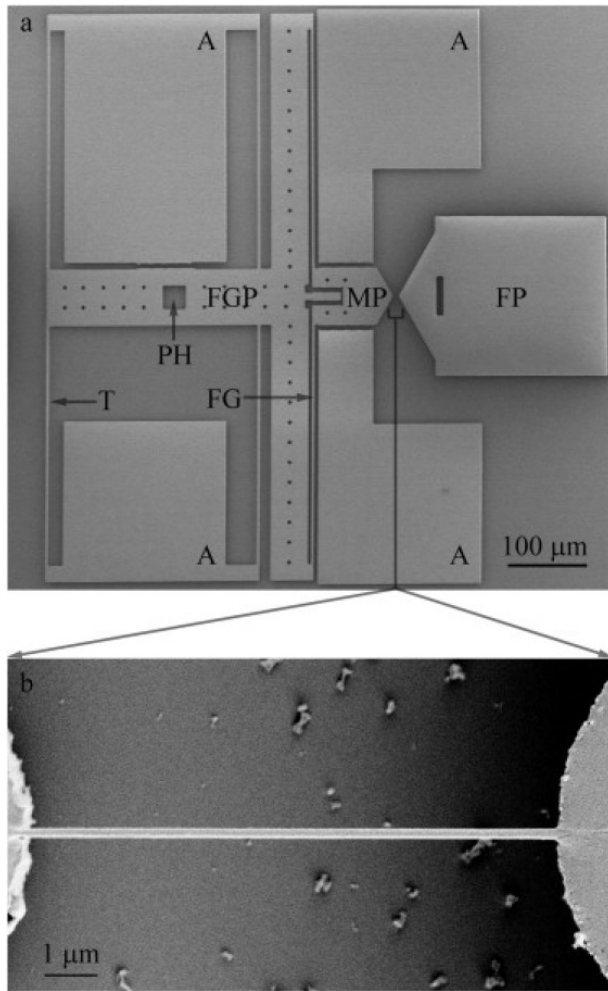


Fig. 1.8: (a) Diagram showing different parts of a MEMS device for tensile testing experiment which consists of a fixed pad (FP), a force-gauge pad (FGP), a movable pad (MP), four tether beams (T), four anchor pads (A), a force gauge (FG) and a pushing hole (PH) (b) SEM image of a single fibril. Figure adapted from⁸²

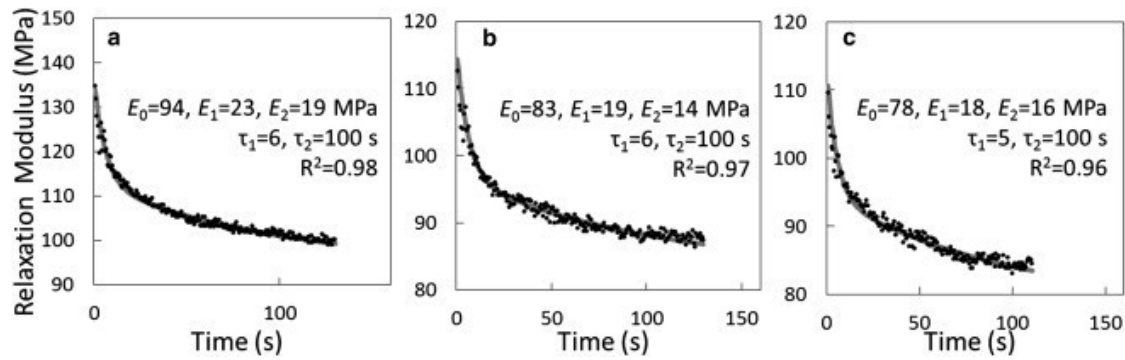


Fig.1.9: Stress vs. time plot that showed viscoelastic response of collagen fibrils for three tests, the Elastic moduli and the relaxation times from the experimental data was obtained by fitting the curves with Maxwell-Weichert model. Figure adapted from⁸²

1.6 Research Questions

Based on my review of the literature I have identified 3 questions in the field of mechanically induced denaturation of collagen fibrils and tissues.

Q1: Zitnay et al. detected molecular level damage for subfailure loading at the tendon level⁷³, Is the observed molecular damage at low tendon strain due to strain localization at the fibril level or does molecular damage occur even at low strain at the fibril level ?

Q2: What is the mechanical energy necessary to unfold collagen molecules within a stretched fibril?

Q3: Yang et al. and Shen et al. studied the stress relaxation mechanism in single collagen fibrils^{77,82}, What is the impact of stress relaxation on molecular unfolding in a single collagen?

Chapter 2

Materials and Methods

2.1 CDET collection, collagen fibril extraction and sample preparation

The fresh forelimb of an adult steer (18-24 months old) was harvested from a slaughterhouse (East Meats, NS, Canada) and brought to laboratory for dissection. Using a scalpel and tweezers, the forelimb was opened up at room temperature and the CDET was identified between the MDET (medial digital extensor tendon) and LDET (lateral digital extensor tendon). The non-tendinous materials were removed carefully and the CDET was extracted from the forelimb. The tendon was then cut into few pieces (each 3-4 cm, convenient size for fibril extraction) on the day of collection, wrapped in gauze soaked with Phosphate Buffer Saline (PBS) and stored at -80°C for approximately one month.

In order to extract collagen fibrils, one of the tendon pieces was placed in a plastic dish of radius around 5 cm with 20 mL 1X PBS solution at room temperature. The PBS solution was prepared just before the fibril extraction procedure. To avoid the epitenon and other non-collagenous materials, the central portion of the tendon was selected for fibril extraction. With the aid of razor blade and tweezers, the tendon was sliced longitudinally and the central portion of the tendon was exposed gradually. Once the central portion was exposed, the razor blade was used to scrape. The scraping procedure was continued for 15 minutes to extract enough single collagen fibrils into the surrounding PBS solution. The PBS and collagen fibril suspension was then pipetted and distributed in five sample glass dishes of 3 cm radius (2 mL each). The deposited suspension was then placed on a linear shaker table at 1 Hz for 45 min to make sure that the fibrils were

aligned. After shaker table alignment, the dishes were rinsed at least three times with ultrapure water to avoid salt crystallization and dried under compressed nitrogen. Sample dishes were desiccated for 24-48 hours prior to gluing in a desiccating chamber.

2.2 Pulling fine tipped glass rods for gluing purpose

In order to create isolated collagen fibril segments, fine tipped glass rods were produced using a Sutter P-2000 Laser-Based Micropipette Puller (Sutter instrument, USA). The Borosilicate glass capillaries with outer and inner diameter of 1 mm and 0.58 mm respectively (World Precision Instruments, USA) were inserted in the micropipette puller. The CO₂ laser heat source was modulated and directed precisely to obtain a tip diameter from 0.6 mm to less than one micron. I found that the finest pipettes worked best for gluing purposes.

2.3 Isolation of collagen fibril segments and gluing procedure

The detection, isolation and gluing of desiccated fibrils was done using dark field microscopy on an Olympus BH2 optical microscope equipped with a 10X, 0.3 NA objective (Olympus, USA) and WHK 10X/20L microscope eyepieces (Olympus, USA). A fine tipped glass rod was placed on a hydraulic 3D micromanipulator (Siskiyou Corp, USA) and positioned just above the glass surface. A large drop of 5 minutes epoxy mix (Lepage, USA) was placed on one side of the dish and was easily accessible to the glass rod using the micromanipulator.

A moderately dense region of parallel collagen fibrils was selected first and then a single fibril with comparatively clean surrounding was targeted for gluing. The glass rod was moved and dipped into the glue for a few seconds and then it was removed. Excess glue was removed just by pressing the glass rod onto the substrate. Again using the micromanipulator the glass rod was

moved towards the targeted fibrils and two thin glue strips were deposited. We targeted a fibril segment length of around 40-50 μm for gluing (length before gluing) which is compatible with our stretching protocol (Fig. 2.1). However, this was difficult to achieve and we obtained a broad distribution of segment length. In some cases, multiple glue strips were deposited in order to generate multiple segments along the same fibril. After gluing several fibrils this way, in different region of the sample dish, the sample dishes were stored in a desiccator for at least 24 hours before the next experimental step.

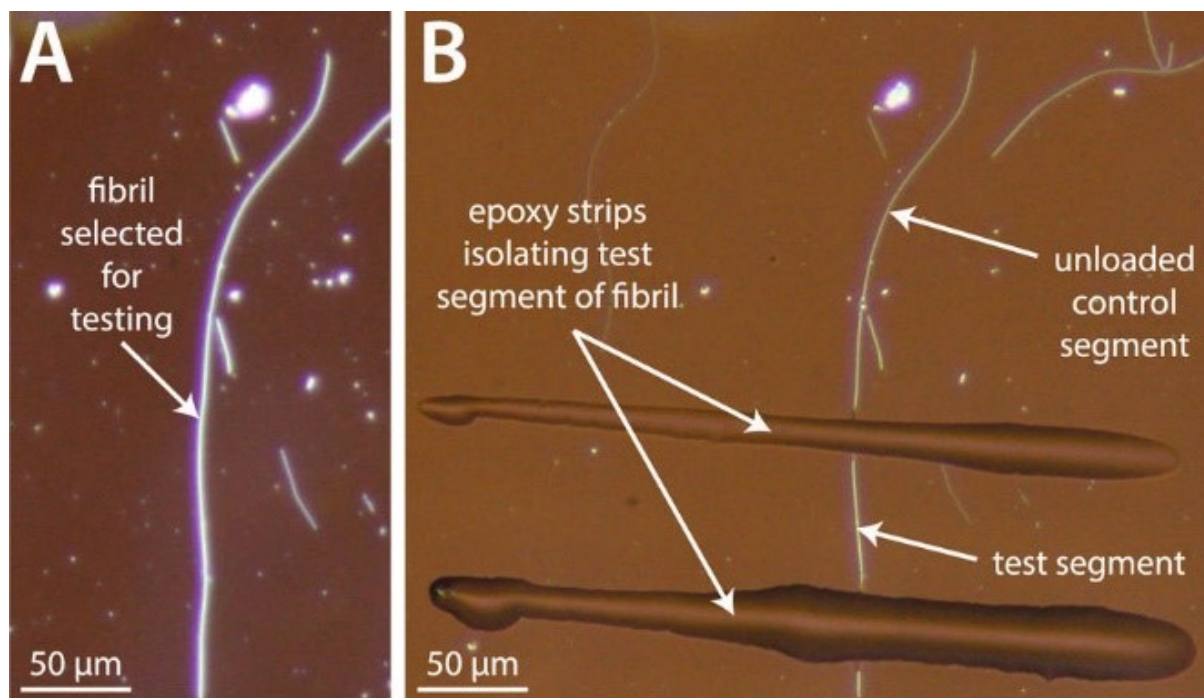


Fig. 2.1: Fibril isolation (A) and gluing (B), brightfield illumination was used in combination with darkfield illumination for better viewing. Figure adapted from⁵⁵

2.4 AFM cantilever characterization and spring constant calibration

Bruker Tap 525A silicon probes (Mean Nominal Spring Constant of 186.5 N/m, standard deviation 5.97, $n=5$) were used for fibril manipulation. The Bruker Tap 525A probe was placed in a probe holder in two different ways so that it was possible to obtain all the dimensions of the probe using a Phenom G2 Pro scanning electron microscope (Phenom-World, Netherlands). The cantilever length, thickness and tip height were then measured in ImageJ to calibrate the lateral force constant of the probes (Fig.2.2). All the dimensions were found within the nominal range ($115 < L < 135 \mu\text{m}$, $6.0 < T < 7.5 \mu\text{m}$, and $15 < H < 20 \mu\text{m}$). In order to measure the normal cantilever sensitivity, the cantilever was engaged on a sapphire sample (Bruker PeakForce QNM Sample Kit) to measure its vertical deflection sensitivity, S_z , by fitting the laser spot deflection on the photodiode with respect to the probe height sensor change. The vertical spring constant K_z was then calculated by combining this with the thermal noise method of Sader et al⁸³.

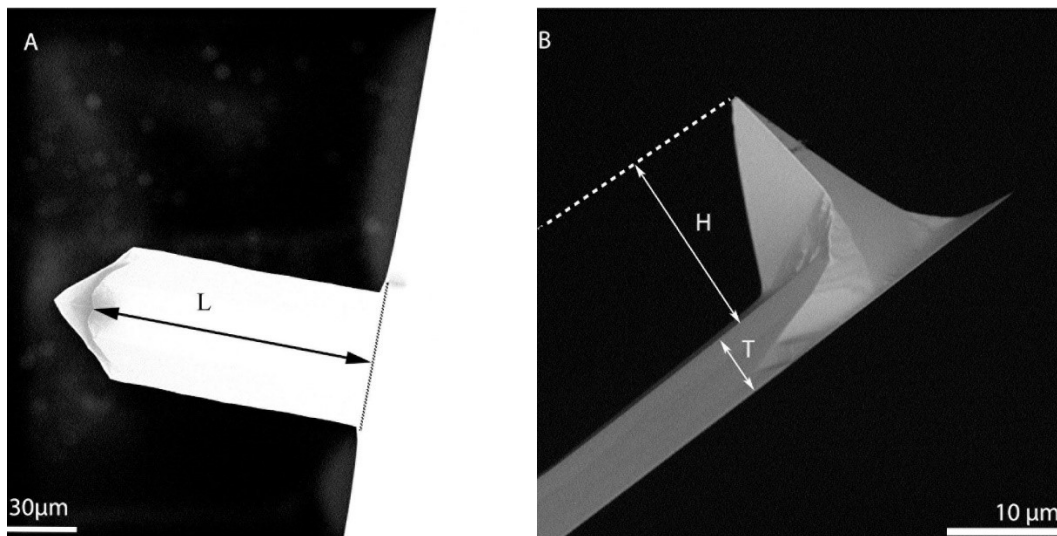


Fig. 2.2: Bruker Tap525A AFM probe viewed under SEM. Images were taken to measure tip length (A), height and thickness (B).

2.5 Pre-manipulated fibril imaging

In order to compare the morphology of the pre- and post-manipulated fibrils, AFM imaging of the dehydrated fibrils was done before pulling using a Bioscope Catalyst AFM (Bruker, USA) in dehydrated condition operating in Peak Force Quantitative Nanomechanical Mapping (QNM) mode. The AFM probe used for fibril imaging was a Bruker ScanAsyst fluid+ AFM probe (nominal spring constant 0.7 N/m). The glued fibrils were detected optically and the AFM tip was engaged at the location. The entire length of the fibril was imaged with a pixel size around 20 nm so that the D-band was visible and with a 0.1 Hz raster scan frequency. The aspect ratio and the angle of scanning were adjusted depending on fibril geometry and imaging time.

2.6 AFM basic operation, experimental set-up and relaxation method

Atomic Force Microscopy is a surface technique in which a probe is scanned across a region of interest while maintaining a constant force. The position of the sample stage and the tip are accurately controlled by the piezoelectric elements, generating a map which can be considered as surface topography. The AFM probe is a pyramidal tip attached to a flexible cantilever. The deflection of the cantilever is measured using a laser focused on its back and a photodiode.

In this study, the sample manipulation was done in contact mode and imaging was done in tapping mode. As the name indicates, in contact mode, the AFM tip remains in contact with the sample and enables lateral manipulation of the sample keeping the normal deflection of the cantilever constant. On the other hand, in the tapping mode, the AFM tip oscillates in and out of contact maintaining constant oscillation amplitude.

The relaxation experiment and fibril imaging were accomplished using Bioscope Catalyst AFM (Bruker, USA) mounted on an inverted microscope (IX71, Olympus, USA). First the sample dish was rehydrated with 3ml of PBS for 30 min. The sample dish was kept on the AFM stage for manipulation in such an orientation that the longitudinal fibril axis was parallel to the axis of the AFM cantilever (Fig. 2.3A). The laser reflected from the back of the cantilever was collected on a four quadrants photodiode, the output of the photodiode controlled the tip-sample distance through a feedback loop (Fig. 2.3A). The fibrils were pulled in bowstring geometry⁵⁶. (Fig. 2.3B). The pulling velocity was 1 μ m/sec with a straight path going through the middle of the fibril. During pulling, the normal applied force was maintained around 40 μ N. The feedback loop gains were set to an integral gain of 1.4 and a proportional gain of 5.0 as this combination limited the occurrence of the cantilever hopping over the fibril. The lateral deflection of the cantilever versus time was acquired during the entire fibril manipulation at a frequency of 500Hz. After pulling the fibril up to a given strain, the probe was stopped and held in place for a specific time (1-1500 sec times), and then the probe was lifted off the surface to allow the fibril to relax back to its initial position. Optical images of the fibrils were also captured during the whole process at the rate of 5 fps with a CCD camera (Grasshopper Point Grey, Canada) and a magnification of 100X in differential interference contrast (DIC) mode.

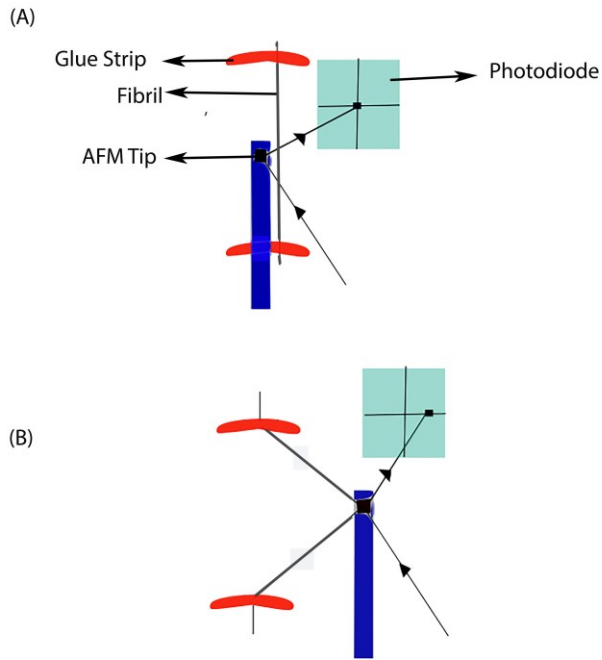


Fig.2.3: (A) A simple illustration of the bowstring geometry and (B) basic AFM operation

2.7 Overview of relations between mechanical parameters

During the manipulation process the AFM tip contacts the fibril which causes a lateral deflection of the laser beam on the photodiode. The lateral force was computed by the relation^{84,85},

$$F_{lateral} = S_z K_z L V_{lateral} / (1 + \nu) (H + \frac{T}{2}) \quad (1)$$

Where, $S_{lateral}$ [nm/V] is the lateral sensitivity, $K_{lateral}$ [N/m] is the lateral spring constant, and $V_{lateral}$ [V] is the lateral voltage deflection. L, H and T are defined in Fig. 2.2, S_z is the vertical sensitivity, K_z is the vertical spring constant and ν is the Poisson's ratio (0.27) for silicon⁸⁶.

Depending on the Fibril-probe contact point and fibril alignment with respect to the cantilever long axis, we have three cases for bowstring geometry (Fig. 2.4A-2.4C). The maximum strain achieved was measured optically for each fibril.

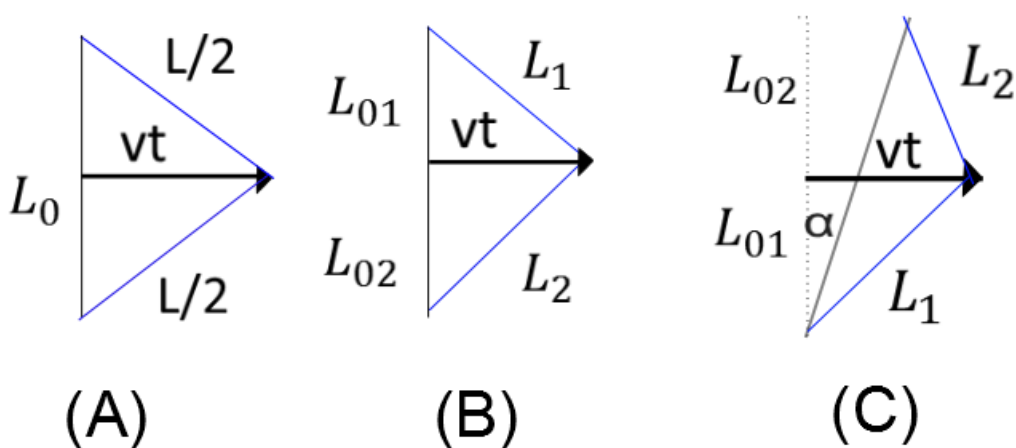


Fig. 2.4: (A) Bowstring geometry where AFM tip pulled through middle point, two sides of the fibril achieved similar strain. (B) Fibril was pulled asymmetrically, uneven strain produced. (C) Fibril axis was not perfectly parallel to AFM tip, therefore pulling angle was taken into account.

For each fibril manipulation the lateral defection voltage-time curve was converted to a force-time curve using equation (1) and was correlated with the captured video. The raw force data was smoothed using a window size of 20 points. Fig. 2.5 A is an example of an entire force-time curve from first contact between the tip and the fibril (the fibril feels tension from point a), pulling to maximum strain (point b) followed by force relaxation for 150s. Fig. 2.5 B is a close-up of the pulling region showing that a sharp increase is observed after the fibril fully detached from the substrate at around $5\mu\text{m}$. The force relaxation happened in two phases, a fast

decrease (until point c in Fig. 2.5 A) and a slower average decrease with large oscillations until the end (point d in Fig. 2.5 A). During the force relaxation part of the experiment it was common for the force to become negative compared to the force at first contact indicating that the fibril force relaxation is not the main driver of the lateral deflection of the cantilever beyond point c (Fig. 2.5 A). After holding the fibril for 150s, the AFM tip was released and the fibril came back close to its initial position without any evidence of rupture (Fig. 2.6 C).

In order to calculate the total mechanical energy to stretch the fibril, Force-displacement curve like Fig. 2.5 (B) was generated. The whole force-time curve was then integrated to calculate the total mechanical energy given in the system.

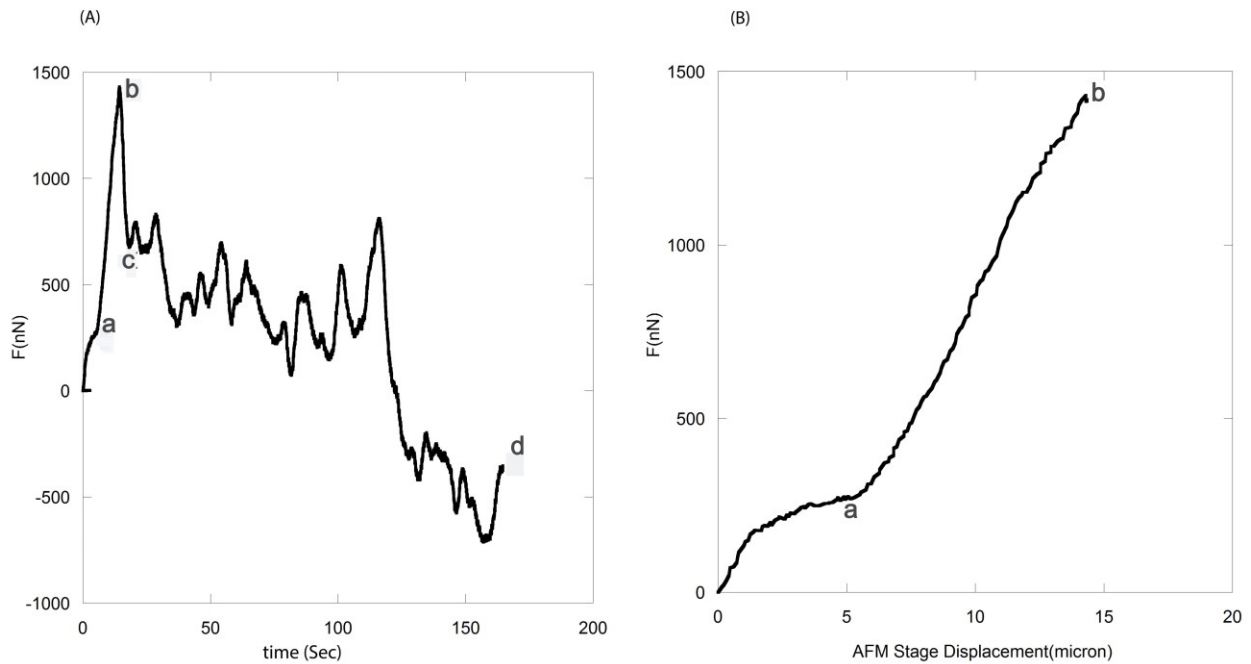


Fig. 2.5 (A & B): Transformation of voltage-distance curve to Force-time and Force-distance curve.

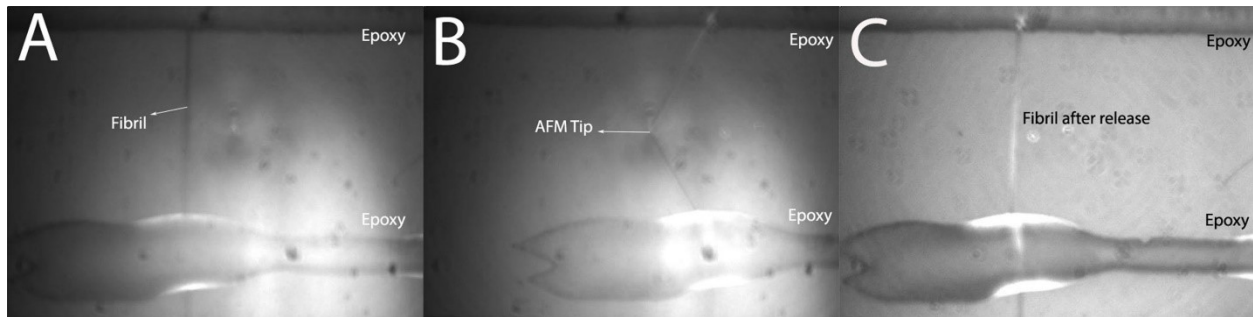


Fig. 2.6 (A-C): Pulling sequence, the fibril was pulled by the AFM tip (17% strain) and was held for a particular time period.

2.8 Post-manipulated Fibril imaging

After the relaxation test of all the fibrils in the dish, the PBS solution was removed from the glass dish, and the dish was rinsed at least three times with ultrapure water. The sample dish was then dried under compressed nitrogen and stored again in the desiccating chamber. After 12 hours, the post-manipulated AFM imaging was performed with Bruker ScanAsyst fluid+ AFM probe Catalyst AFM (Bruker, USA). The imaging technique and parameters used were kept exactly the same as for pre-manipulation imaging for direct comparison.

2.9 Sample preparation for post-manipulated fluorescence imaging and fluorescence imaging protocol

The sample dishes containing the fibrils were rehydrated with 3 ml ultrapure water for an hour. 10 μ M Fluorescein conjugated collagen hybridizing peptide (CHP) (Echelon Biosciences Inc., Salt Lake City, UT) solution was prepared at room temperature under normal lab environment. The peptide solution was heated at 80°C for 5 min in a dry bath incubator and cooled by immersion in an ice bath for 15 seconds. The ultrapure water was dumped from each dish, replaced by 2

ml of the cooled peptide solution and the dishes were incubated at 4°C for 12 hours. The peptide solution was removed and each dish was rinsed 3 times with ultrapure water, five minutes per rinse. The dishes were dried under compressed nitrogen for few minutes, covered in aluminum foil and kept in the dark until fluorescence imaging was performed.

Fluorescence imaging was performed on a Zeiss LSM 710 upright confocal microscope equipped with a 488 nm Argon laser. Samples were imaged with a 40X oil immersion lens with digital zooms of 2.0X and 5.5X. A region of interest (ROI) function was employed for isolating manipulated fibrils from the rest of the sample for scanning and imaging. Micrographs were obtained with ZEN 2009 Microscope and Imaging Software. Laser scanning and bright field images were acquired as a stack for each ROI.

2.10 Data Analysis

2.10.1 Fibril height profiling

Height was taken across the length of the fibril from the AFM image of pre- and post-manipulated fibril to probe change occurring due to stress relaxation. The height image was launched in SPIP image analysis software, was flattened, zoomed and then a segmented line was drawn manually from one end of the fibril to another through its middle (Fig. 2.7A). The glue droplets at the two ends were avoided during the height profiling. The height was always taken from the same end of each fibril so the generated profiles from pre- and post- manipulated fibril were directly comparable.

2.10.2 Fibril cross section profiling

In order to see changes in width as well as height, the cross section mapping of the fibril was required. Cross-sections were taken approximately at each micron interval along the length of the fibril (Fig. 2.7 B) and therefore a cross-section profile for pre- and post- manipulated fibril was made for comparison. The fibril height image was launched in SPIP, flattened and zoomed first. Then a line was drawn at the one end of the fibril (avoiding glue droplets) perpendicular to fibril length. The generated profile was opened in Kaleidagraph and the selected area was integrated (Fig. 2.8). The cross section obtained from each point was then plotted against the distance along the fibril, which generated cross section profile of pre- and post- manipulated fibril.

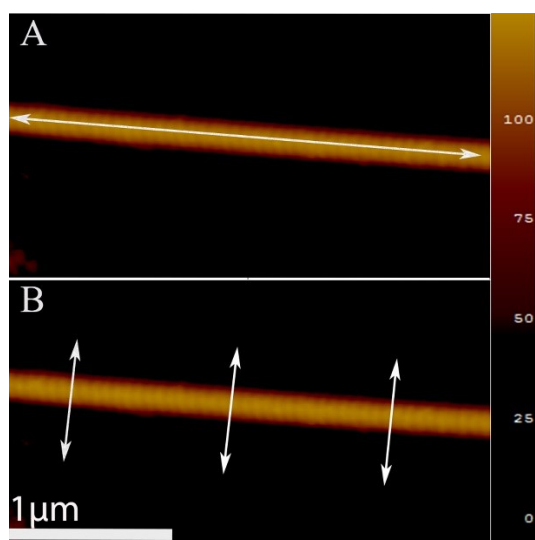


Fig. 2.7: (A) Height profiling and (B) Area profiling of fibril before and after manipulation. The height profile was taken along the length of the fibril where cross-sectional area was measured at certain location perpendicular to fibril length, approximately every micron interval.

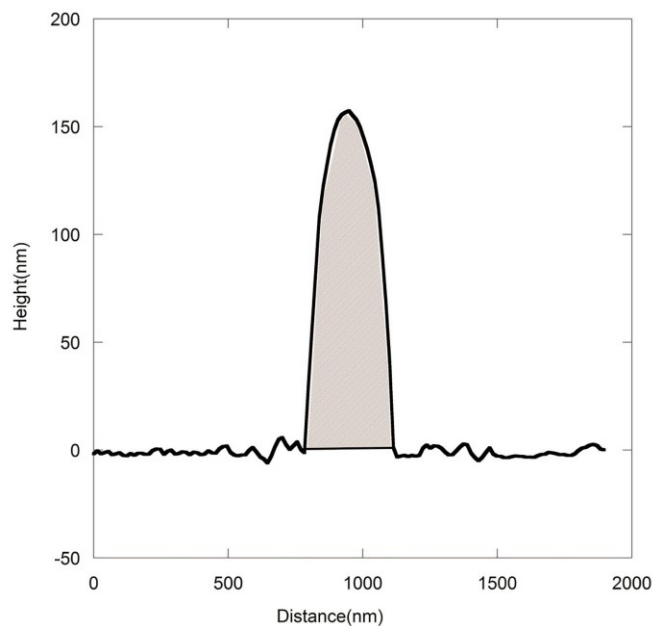


Fig. 2.8: Example of height-distance profile at each location where cross section of the fibril was measured. The shaded region was integrated for estimating area.

2.10.3 Fluorescence Intensity Profiling

Fluorescence intensity mapping was done on all manipulated fibrils in order to quantify the extent of molecular damage accrued during fibril manipulation. The brightfield image was opened in ImageJ, a line with a width of typically 5 pixels (through the middle of the fibril, comparable to fibril width) was drawn across the length of the fibril. Then keeping the line at the same location, I switched to the fluorescence image, which gave fluorescence intensity profile. The background fluorescence was measured by moving the line 5-10 microns away from the fibril. The obtained profile of fluorescence intensity profile was then subtracted from the background and smoothed over 20 data points.

2.10.4 D-Band Measurement

The height profile acquired was separated for all the cases where the strain was not similar on both sides, the data was interpolated with 2048 pixels and FFT was performed. The peak was visible around 0.015 nm^{-1} corresponds to D-band signal, this peak was fitted with Gaussian to get D-band measurement.

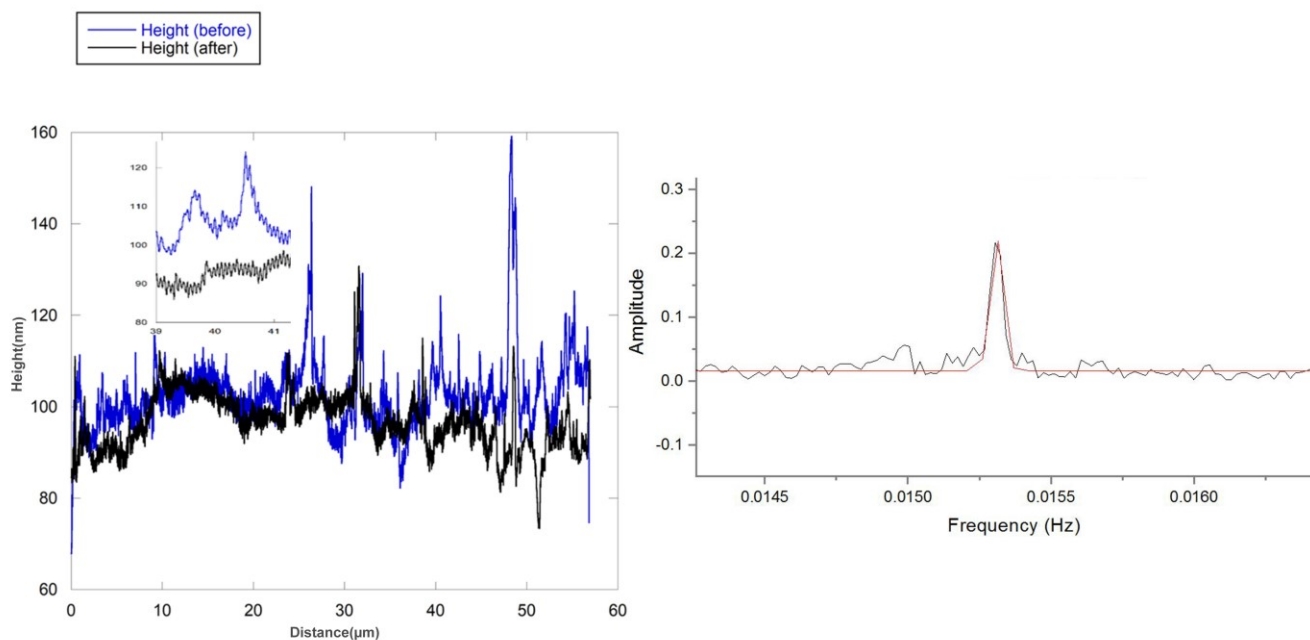


Fig. 2.9: (A) Example of height profile of the fibril along the length before and after manipulation, portion of the profile height has been zoomed in inset (B) FFT of the profile, the peak has been fitted with Gaussian to measure D-band.

2.10.5 Statistical Analysis

Average \pm standard deviation has been presented in each bar graph. One-way ANOVA was performed in SPSS and Kaleidagraph in order to check whether there is an overall statistically significant difference between multiple groups exists or not. Based on the result of ANOVA test, Fisher's LSD post hoc was performed to calculate significant difference between each group. Students unpaired t-test was performed in case of comparing only two groups. In bar graphs, we have used following notation to mention the significant difference: * $p < 0.05$, ** $p < 0.01$, *** $p < 0.001$. For linear trends, the significance of the linear fit has been reported based on the ANOVA result of linear regression test in SPSS.

Chapter 3

Results

A bowstring stretching and relaxation protocol was applied to 14 collagen fibrils extracted from the CDET of one bovine steer forelimb. 6 fibrils were pulled symmetrically (Fig. 2.4A) and 8 fibrils were pulled asymmetrically (Fig. 2.4B and 2.4C) yielding 22 fibril segments considering symmetric cases as one segment since these fibrils experienced similar strain (less than 2% strain difference) on both sides. In addition, one fibril went through the same preparation as the other ones but was not manipulated and served as a control. After the fibrils were stretched and relaxed for different times, the AFM tip was lifted up to release the fibrils. In all 14 cases, the fibril came back close to its initial position without breaking (Fig. 3.1) and within the time of one video frame, 200 ms. This proves that all the fibrils were under tension at the end of the relaxation period even so the force measured at the tip became negative during relaxation (Fig. 2.5A). Due to this limitation the force relaxation curves were not analyzed and I focused on morphological and molecular changes due to the manipulation protocol.

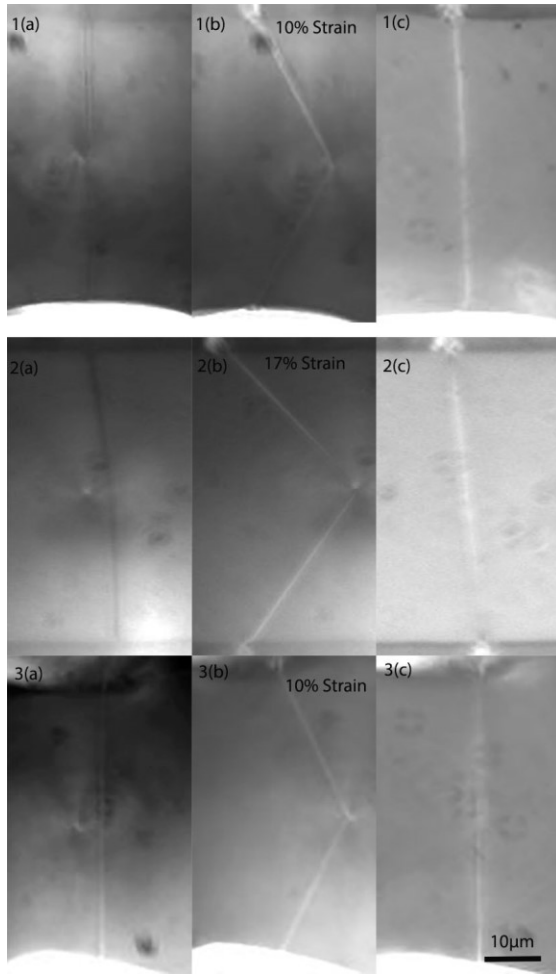


Fig. 3.1: Optical microscopy frames taken before manipulation, at the maximum strain and after release for the three relaxation times, 1s (1a-1c, 1st row), 150s (2a-2c, 2nd row) and 1500s (3a-3c, 3rd row). The change in brightness of the fibrils after release may be due to water uptake.

3.1 Collagen fibrils morphology and supramolecular structure before and after manipulation

The fibrils were stretched between 4% and 22% and were held at the target strain for three different relaxation times, 1 second ($n=5$, where n is the number of fibril segments), 150 seconds ($n=13$) and 1500 seconds ($n=4$). The fibrils had a broad distribution of test segment length (23-69

μm), mean dry height (75-169 nm) and mean dry cross-sectional area (17,000-50,000 nm^2) before manipulation. The values for these parameters varied as well between the fibrils exposed to the three different relaxation times (Table 3.1).

Relaxation time (s)	Number of fibrils	Mean length (μm)	Mean height (nm)	Mean cross-sectional area (nm^2)
1	3	31 \pm 8	143 \pm 13	44,000 \pm 5,000
150	8	50 \pm 17	122 \pm 26	31,000 \pm 12,000
1500	3	31 \pm 10	149 \pm 12	44,600 \pm 1000

Table 3.1: Collagen fibrils morphology before manipulation (measured value \pm SD) for each relaxation time.

Height and cross-sectional area profiles of all the fibrils studied (before and after manipulation) including the control fibril showed noticeable variations along the length. As an example, the control fibril height and area profile are presented in Fig.3.2 A&B. The fibril was not manipulated but appeared to swell after the second drying step indicating that the humidity in the room was not constant throughout the experiment. The mean dry height of the fibril is 133 \pm 11 nm, with a coefficient of variation of 8% while the mean dehydrated height of the fibril after the second dehydration step is 143 \pm 12 nm, with almost the same coefficient of variation. The cross-sectional area profiles showed a bit more variation (coefficient of variation of 10% and 13% for first and second profiles respectively) with mean dry cross-sectional area 40,000 \pm 4,000 nm^2 (first dehydration step) and 46,000 \pm 6,000 nm^2 (second dehydration step).

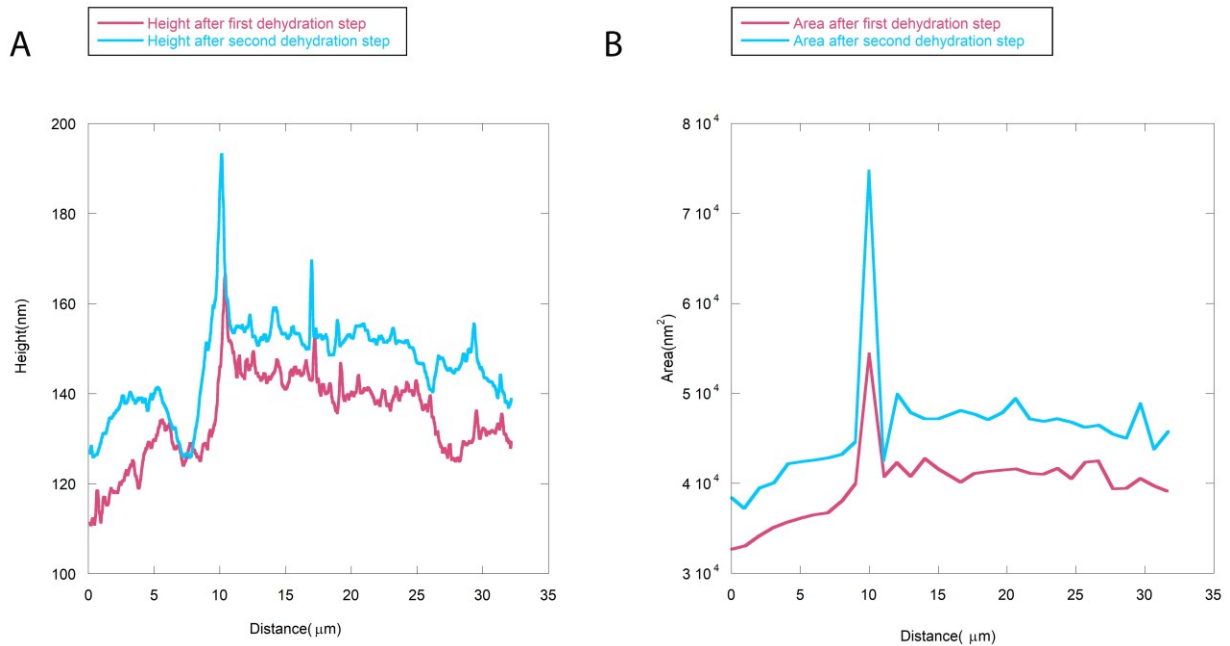


Fig. 3.2: (A) Height and (B) Cross-Sectional area profile of the control profile, the shape of both height and area curve remained similar.

The change in mean height and mean cross-sectional area of all the manipulated fibrils, pooled by relaxation time, is presented in Table-3.2. Half of the fibrils showed an increase in height after relaxation while only two fibrils swelled in cross section after manipulation. The average height change for all fibrils into consideration is always small, around $9 \pm 5\%$, while in case of area the change is about $11 \pm 6\%$. No significant change has been observed in total length of the fibril due to manipulation.

Relaxation time (s)	Number of fibrils	Absolute change in mean height (nm)	Absolute change in mean cross-sectional area (nm ²)
1	3	11±6	5000±2800
150	8	10±7	3000±1700
1500	3	14±7	2200±1300

Table 3.2: The morphological change in fibril after relaxation (measured value \pm SD), for each relaxation time.

The supramolecular structure of the fibrils, as assessed by the D-band spacing characteristic of the staggering pattern of the collagen molecules, was insensitive to the manipulation protocol. The mean difference of D-band spacing before and after manipulation for all fibrils is effectively zero, 0.02 ± 0.94 nm (Fig. 3.3A). The D-band spacing decreased by no more than 2 nm for half of the manipulated fibril segments while the other half showed no more than a 2 nm increase (Fig.3.3B). Pooling the fibrils per relaxation time did not change this picture (Table 3.3) indicating that the supramolecular structure of the fibrils seems unaffected by the bowstring stretching and relaxation protocol for all strains between 4 and 22%.

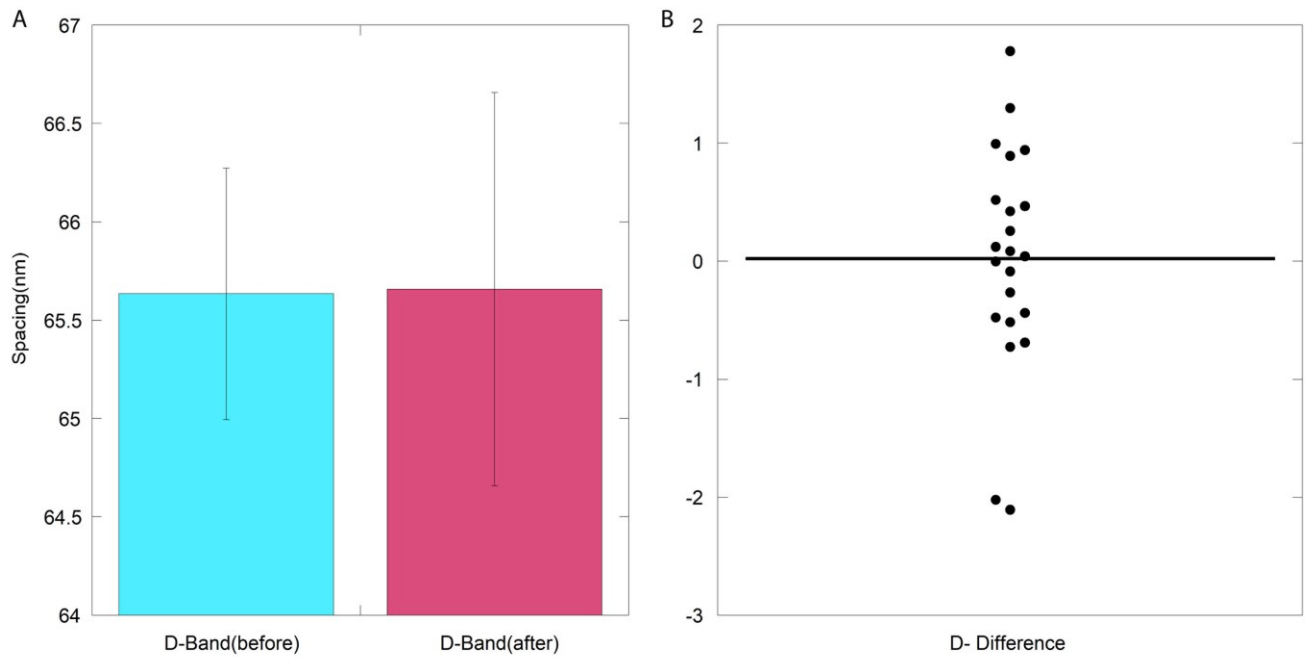


Fig. 3.3: (A) The mean D-band spacing before and after manipulation (B) Distribution of D-band difference (nm).

Relaxation time (s)	D-band (before, nm)	D-band (after, nm)	D-band difference (after-before, nm)
1	65.63±0.64	65.08±1.44	0.55±0.9
150	65.62±0.75	65.85±0.69	0.23±0.86
1500	65.67±0.28	65.74±1.25	0.07±1.17

Table 3.3: Summary of D-band measurements for each relaxation time.

3.2 Tensile loading and release lead to molecular denaturation

The bowstring stretching protocol followed by relaxation for up to 1500 s yielded no significant change in supramolecular structure of the collagen fibrils as assessed by the D-band spacing. However, this result does not rule out the possibility that portions of the collagen molecules unfolded due to tensile loading, stress relaxation and/or instantaneous release. In order to check this possibility, we used CHP that binds specifically to denatured collagen triple helices and is widely used for the detection of molecular unfolding or damage in collagen⁷⁰⁻⁷².

The fluorescence image analysis of the CHP treated manipulated fibrils revealed molecular denaturation. The background corrected fluorescence intensity profile along each CHP treated fibril was extracted from the fluorescence image, and the mean intensity was measured. The regions within 1 micron of the glue attachments and the tip contact point were excluded from this analysis. Fig. 3.4 summarizes the distribution of mean fluorescence intensity for the three different relaxation times, averaging over all strain levels. The control segment showed minimum intensity compared to the three manipulated groups. There is an apparent increase of mean fluorescence intensity with increasing relaxation times (3.56 ± 1.01 , 3.82 ± 1.41 and 4.58 ± 1.88); However, one-way ANOVA tests and Student-Newman-Keuls post hoc tests showed no significant difference between these three groups.

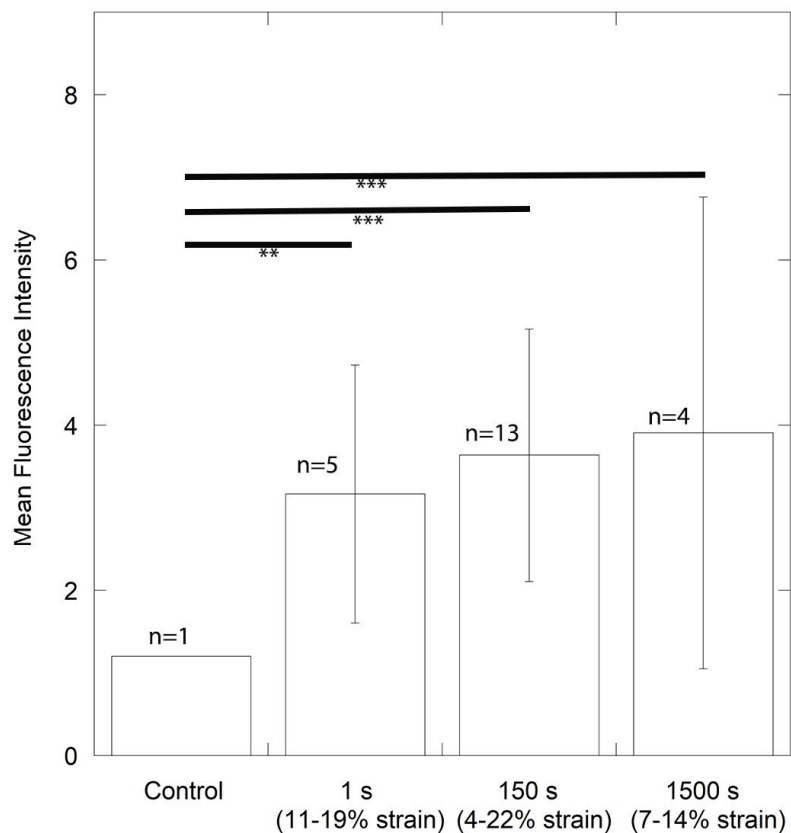


Fig. 3.4: Mean fluorescence intensity along the fibrils for the control case and the three relaxation times. The range of strain within each group is indicated in parenthesis. There was a significant difference between the control case and the three manipulated groups.

3.3 Fluorescence intensity profile for different strain levels

The fluorescence intensity varied notably within the same fibril when it experienced two different strain levels (asymmetric cases, fig. 2.4B & 2.4C). As an example, Fig. 3.5 shows the fluorescence profile and fluorescence image of a fibril strained asymmetrically to 5 and 20% strain. There is a visible increase in fluorescence intensity going from the low strain to the high strain region along the profile. All fibrils that experienced asymmetric stretching showed the same behavior

independent of relaxation time, Fig. 3.6 provides all eight cases asymmetric cases. Unpaired t-test was performed on the mean fluorescence intensity between the high strain and low strain region of each fibril that experienced asymmetric stretching and six cases were statistically significant.

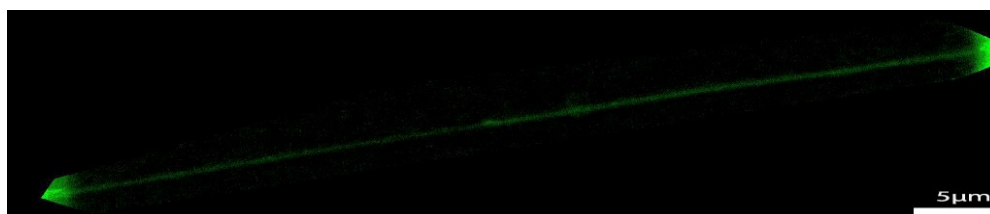
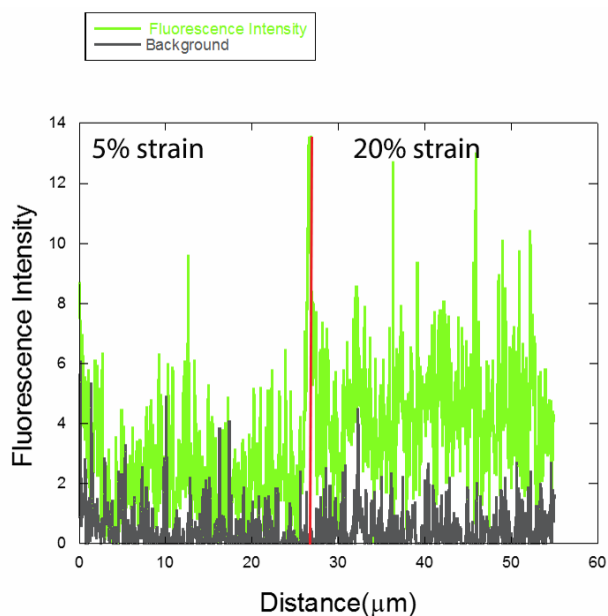


Fig. 3.5: An example of fluorescence intensity profile and corresponding fluorescence image with enhanced contrast (corresponds to Fig.3.6A) where the fibril experienced two different strains, 5 and 20% on each side and showed different fluorescence intensity level. This fibril was exposed to a 150 s relaxation before release.

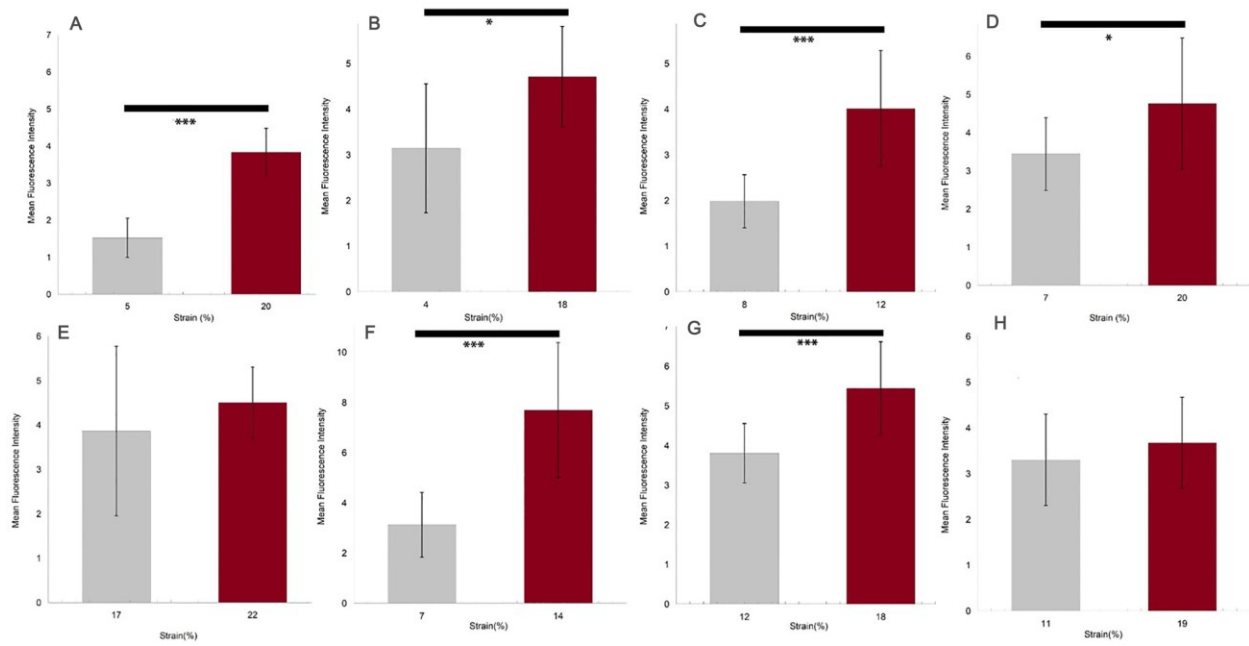


Fig 3.6: Mean fluorescence intensity between the low strain and high strain region of all the fibrils that experienced asymmetric stretching. (A-E) 150 s relaxation time, (F) 1500 s relaxation time and (G,H) 1 s relaxation time, six strain pairs showed statistically significant difference in unpaired t-test.

In addition, we observed that the difference in observed fluorescence intensity between the two sides of the same fibril was independent of the strain difference (Fig. 3.7).

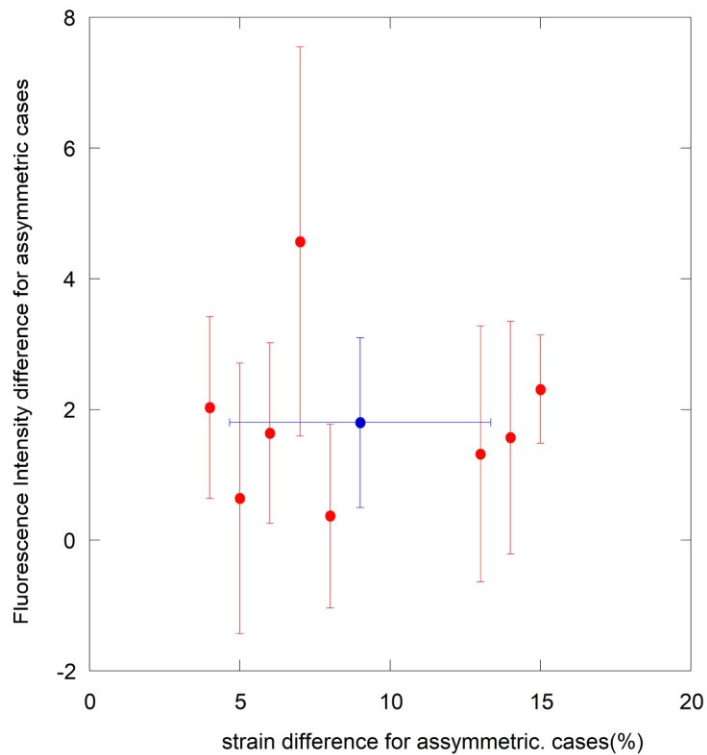


Fig 3.7: Plot of strain difference and fluorescence difference for asymmetric cases, blue dot represents average and standard deviation of all data points.

3.4 Fluorescence Intensity and Strain dependence

Even so we did not find any evidence of linear dependence of fluorescence intensity difference with strain difference for the asymmetric cases, we wanted to explore whether there is correlation between the mean fluorescence intensity of each segment and the strain it experienced. In order to relate these two variables, we plotted mean fluorescence intensity against the strain applied (Fig. 3.8A) for all three relaxation time categories. The fluorescence intensity of the control fibril is presented as well for comparison but not included in the following analysis. All the manipulated fibrils showed a higher level of fluorescence intensity compared to the control, as expected (Fig. 3.4). All the data points were analyzed together, ignoring relaxation

times (Fig. 3.8A), and the two quantities were found to be linearly correlated ($P=0.023$, see dotted line). Linear fits for each relaxation time are also presented in Fig. 3.8A, however the only statistically significant case corresponded to a relaxation time of 150 s ($P=0.03$). Taking into account the reported stress-strain curves of CDET fibrils that show a stress plateau starting around 10-15% strain^{55,57}, we have categorized the mean fluorescence intensity into four groups (Fig. 3.8B), Significant difference was found between the low strain group (<10% strain) and both intermediate (10-15% strain) and high (>15%) strain groups. However, the intermediate and high strain groups showed no significant difference. The control and low strain groups were not statistically different as well. These results indicate that the physical relationship between fluorescence intensity and strain is not linear (Fig. 3.8B), instead there seems to be two fluorescence intensity levels with a threshold strain around 10%. This idea is supported by the absence of correlation between the difference in fluorescence intensity and the strain difference observed for the asymmetric cases (Fig. 3.7). In most of these cases the two segments were subjected to strains above and below 10%, respectively (Fig. 3.6) and the average fluorescence intensity difference is around 2 units in agreement with the difference in mean fluorescence intensity between the Low strain and Intermediate strain groups in Fig. 3.8B. Furthermore, we have indirect evidence that the fluorescence intensity may be modulated by the applied stress above and below the strain threshold. This idea is supported by the fact that the coefficient of variation (CV) of the fluorescence intensity increases with the coefficient of variation of the cross-sectional area of the fibril before manipulation for all manipulated fibrils (Fig. 3.9). The intrinsic fluctuation in cross-sectional area along the length of the fibril therefore may have some impact on the observed spatial fluctuation in fluorescence intensity. Fig. 3.10 shows one example of

observed fluctuation in cross-sectional area before manipulation and fluorescence intensity at every micron length of the fibril; the spatial fluctuations are fairly negatively correlated between the two profiles albeit with different scales (CV= 0.05 and 0.7 for area before manipulation and fluorescence profile, respectively).

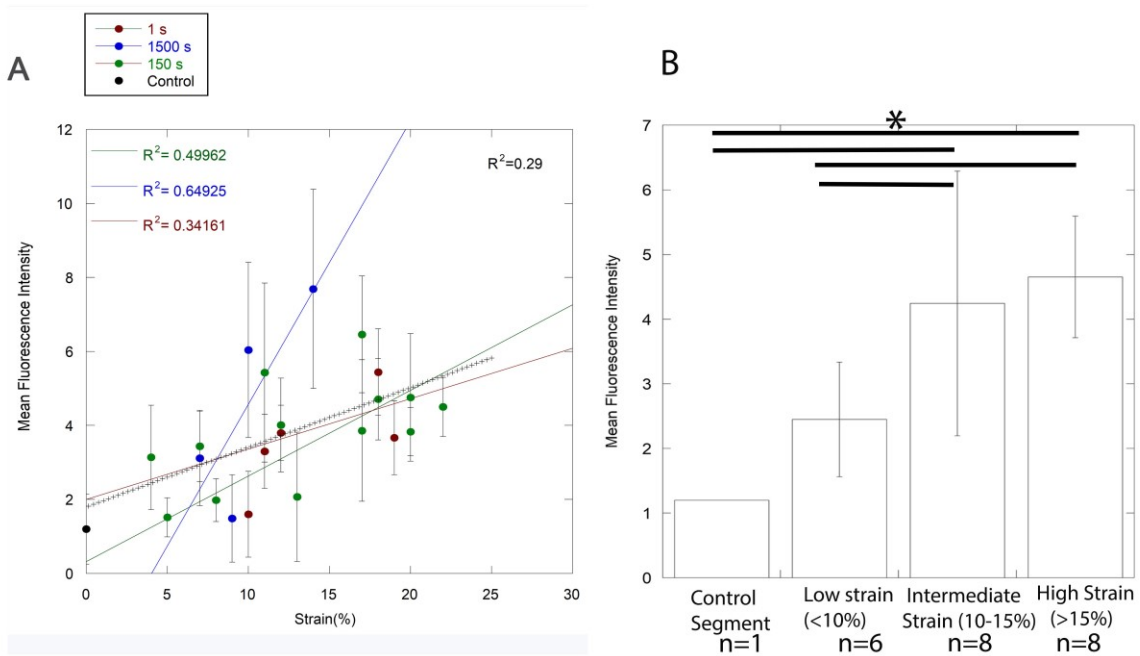


Fig. 3.8: (A) Relationship between fluorescence intensity and the strain applied on each fibril for the three different relaxation times (B) Strain categories introduced based on the typical stress-strain curve of CDET fibrils^{55,57}. One-way ANOVA tests indicated significant pairwise differences in mean fluorescence intensity between the control and the intermediate and high strain groups, the same was true for the low strain group.

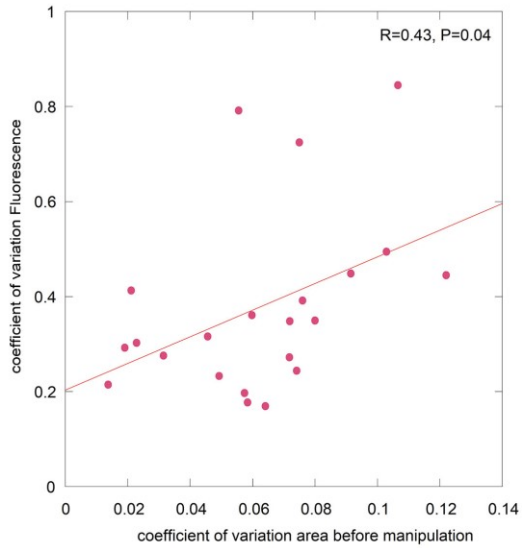


Fig.3.9: Relation between coefficient of variation of fluorescence and coefficient of variation of area before manipulation, statistically significant linear trend has been found in linear regression analysis.

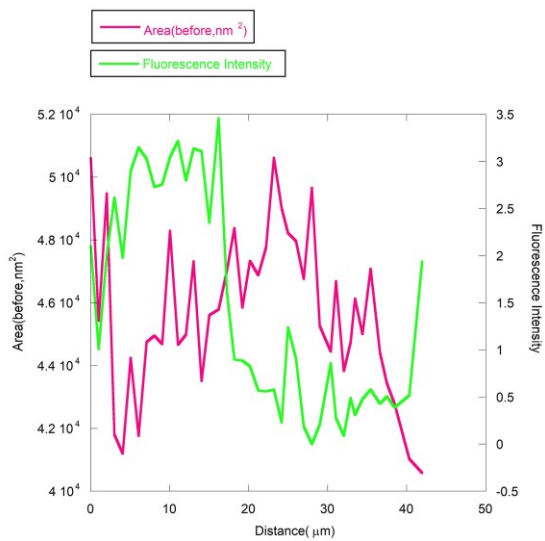


Fig. 3.10: Pre-manipulated fibril cross-section and corresponding fluorescence intensity at every micron length. The fluctuation is clearly visible in both profiles.

3.5 Relation between observed fluorescence intensity and fibril cross-sectional area loss due to manipulation

The fluorescence intensity measurement of manipulated fibrils showed evidence of CHP binding which in turn indicates denaturation of collagen molecules, keeping the D-band almost intact as shown in table 3.3. During denaturation, the collagen triple helix dissociates into its three strands as pictured in Fig. 3.11⁸⁷. Considering the model in Fig. 3.11 where the triple helix is denatured in its middle, one expects that in the dry state, the central denatured part will collapse onto itself in the absence of water giving rise to a local decrease in cross-sectional area with respect to the triple helical parts of the molecule. This idea is supported by Bozec et al. who proposed that denaturation will cause several phases of conformational changes in collagen fibril, primarily breaking of different intermolecular cross-links and H-bond that stabilizes the molecule leading the collapse of collagen triple helix^{88,89}. Therefore, according to this simple model, the denaturation of collagen molecules within the fibril is then expected to decrease the overall cross sectional area of the collagen fibril. The direct comparison of cross sectional area of fibrils before and after manipulation therefore provides a way to potentially estimate the extent of molecular denaturation due to manipulation. The cross sectional area loss of fibril due to manipulation can be assumed as proportional to cross sectional area loss of all denatured molecules within the fibril, which leads us to hypothesize, that the mean cross-sectional area loss of each fibril will be proportional to the amount of CHP binding and its corresponding fluorescence intensity. Hence, the cross sectional area measurement at every micron along the length of the fibril and its associated fluorescence intensity should be linearly correlated.

In practice, we have observed three kinds of cross-sectional area behavior for fibrils after manipulation, shrinking (90% above, 4 out of 14), swelling (90% and above, 2 out of 14) and combination of swelling and shrinking (8 out of 14) in cross section with evidence of CHP binding for all cases. Fig. 3.12 shows example of two cases, an almost completely shrunk fibril after manipulation and an almost swollen fibril after manipulation. When shrinkage is observed, it is associated with a linear trend between cross-sectional area loss and fluorescence intensity (Fig. 3.12 A, $p=0.001$). When swelling occurs, possibly be due to a difference in humidity conditions before and after manipulation, as already reported by Spitzner et al⁹⁰., there is no correlation between the increase in cross-sectional area and the fluorescence intensity (Fig. 3.12 D). Therefore, in order to get a quantitative idea of molecular denaturation due to manipulation, we focused on the region of a fibril where shrinking was observed and only used cases where a statistically significant linear relationship between cross-sectional area difference and fluorescence intensity was found.

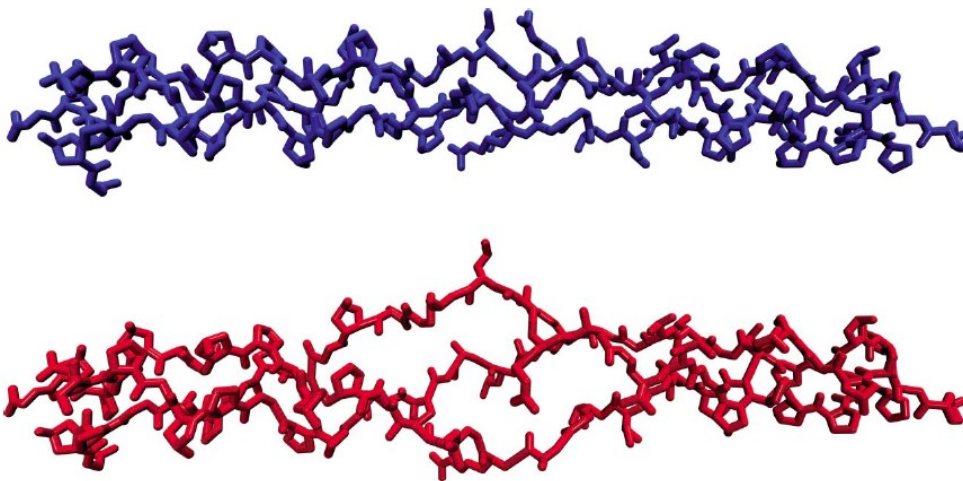


Fig 3.11: Computer simulated “ball and stick” model of collagen triple-helix (top-blue) and denatured state (bottom-red) induced by heat. Figure adopted from⁸⁷

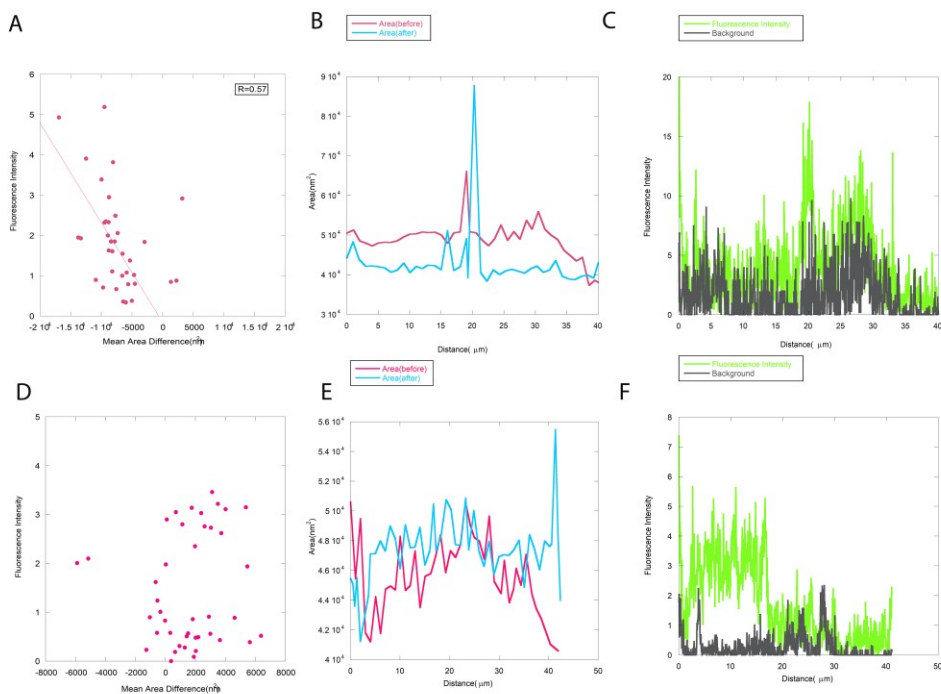


Fig.3.12: Fibril lost area after manipulation, relationship has been shown between mean area loss and fluorescence intensity (A), corresponding area and fluorescence profile before and after manipulation (B, C). Despite of high fluorescence background intensity (C), a clear linear trend has been observed between fluorescence intensity and area loss. An almost complete swollen case, fluorescence intensity has been plotted against mean area difference, area increases despite of manipulation (D, E). The related fluorescence profile before and after manipulation has shown as well (E, F), high fluorescence intensity observed in left side of fluorescence profile with respect to background but no linear or meaningful trend has been found with mean area difference (D, F).

3.6 Quantitative measurement of molecular denaturation due to manipulation

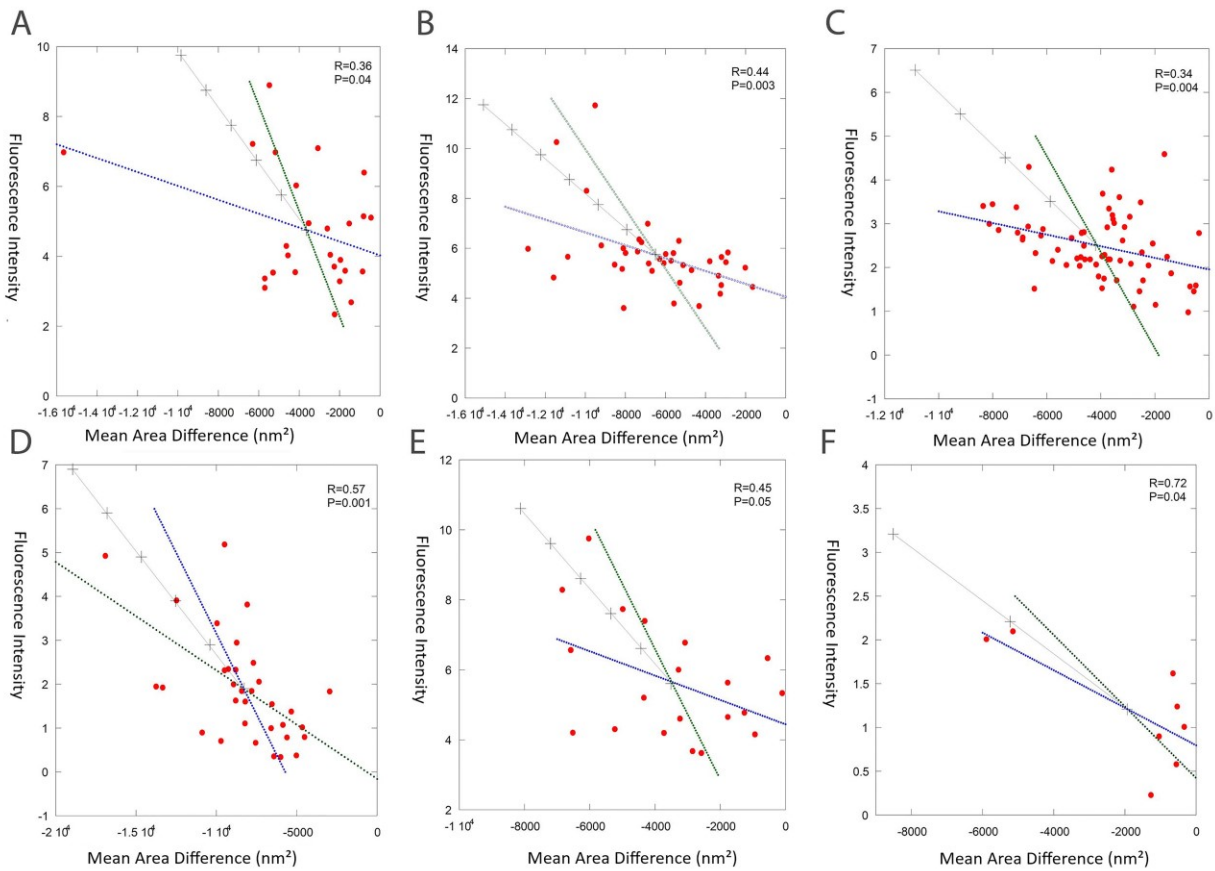


Fig.3.13: (A-F) Cases where statistically significant relationship has been found between mean area difference and fluorescence intensity. The blue colored lines show linear fitting for fluorescence intensity vs. mean area difference, interchanging the axis changes the fitting (green lines). Best line fit has been shown with crossed gray line passing through the intersection of two slopes. In all cases, mean area after manipulation has been subtracted from mean area before manipulation. The strains applied in these cases are 11%, 17%, 11.3%, 10%, 10% and 9% respectively.

Fig.3.13 shows all the statistically significant cases where fluorescence intensity has a statistically significant linear relationship with the cross-sectional area difference. The slope indicates the change in cross-sectional area per unit fluorescence intensity from which we can estimate the number of unfolded molecules per unit fluorescence intensity. Interchanging the axis gave us different slopes (but same P and R-value as indicated in table 3.4), as expected when both variables have large standard deviation, in order to take this effect into account, we have calculated the best fit line slope and corresponding standard deviation with bisector method as proposed by Isobe et al⁹¹. The diameter of a collagen triple helix is 1.1 nm in dry tendon⁹², so the cross section of each collagen triple helix is roughly $0.95 \text{ nm}^2 \approx 1 \text{ nm}^2$ (ignoring the packing fraction calculation). Hence, in order to get an overall and rough quantitative idea of molecular denaturation that took place after stress relaxation, we have considered that the cross-sectional area difference in nm^2 is directly an estimate of the number of denatured molecules per cross-section. Table. 3.4 summarizes all the significant cases, the number of denatured molecules based on that simple assumption, vary widely (the weighted average number of denatured molecules is 1780 ± 625 per Fluorescence intensity unit) which suggests that CHP binding was not uniform across the 7 sample dishes.

Mean Fluorescence Intensity	Slope (arbitrary unit/nm ²)	Slope Error	Calibrated Area Difference (nm ²)	P-value	R-Value	Strain applied (%)	Swelling Percentage (%)
5.43	1241	614	6738	0.04	0.36	11	44
6.46	1432	436	9250	0.003	0.44	17	15
3.96	1668	544	6605	0.004	0.34	11.3	01
1.60	2135	523	3416	0.001	0.57	10	10
6.04	923	434	5574	0.05	0.45	10	25
1.49	3285	1194	4894	0.04	0.72	9	85

Table 3.4: Detailed presentation of fitting parameters of the cases shown in Fig. 3.12 (A-F, respectively), the number of unfolded molecules represent weighted average value of all these slopes and corresponding standard deviation is weighted mean of the error.

Based on the estimated number of denatured molecules per unit fluorescence intensity, we have reconstructed the bar plot shown in Fig 3.8(B) in terms of number of denatured molecules. Fig.3.14 shows the mean number of denatured molecules over the fibril cross-section for the three strain levels introduced previously, there is no statistical difference between the three strain groups due to large standard deviations.

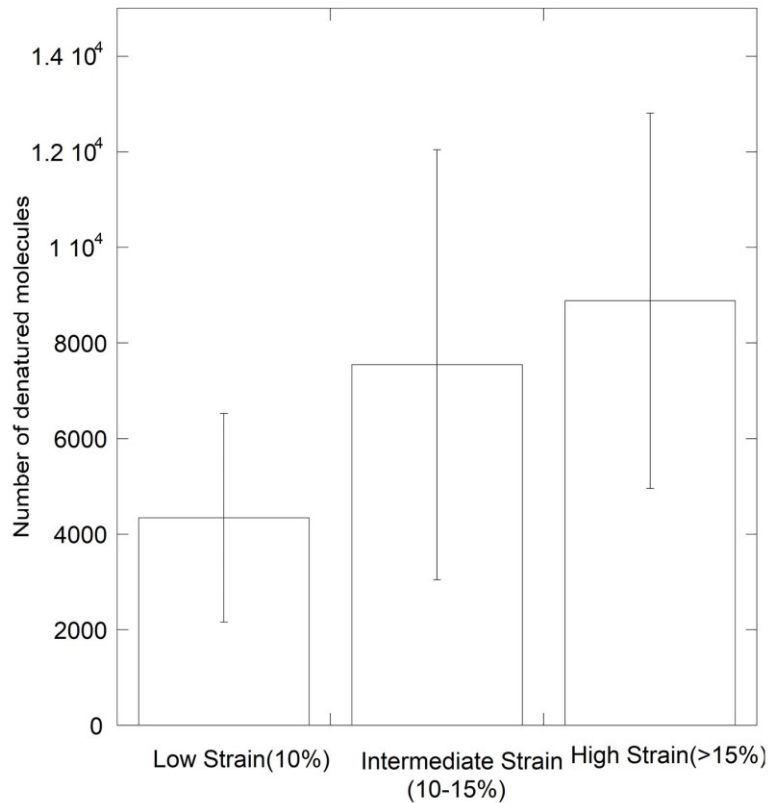


Fig. 3.14: Three strain groups in terms of number of molecules lost due to manipulation based on the calibrated number from the slope presented in table 3.4. The mean number of denatured molecules at high strain group is approximately double than that of low strain group but due to large standard deviations, no statistically significant difference was found.

The mean number of denatured molecules over the cross-section of the fibril is then used to estimate the decrease in fibril dry volume due to manipulation with respect to the initial dry volume. The fraction of volume change, assuming the average change in cross-sectional area estimated holds for the entire fibril including swollen sections, was plotted against the weighted average strain applied in Fig.3.15 (this is to account for the presence of one asymmetric pulling

case). We observed an apparent sigmoidal trend with an onset around 8% strain and we report in average $17 \pm 9\%$ dry volume loss for a strain applied of $11 \pm 3\%$ (blue point in Fig.3.15).

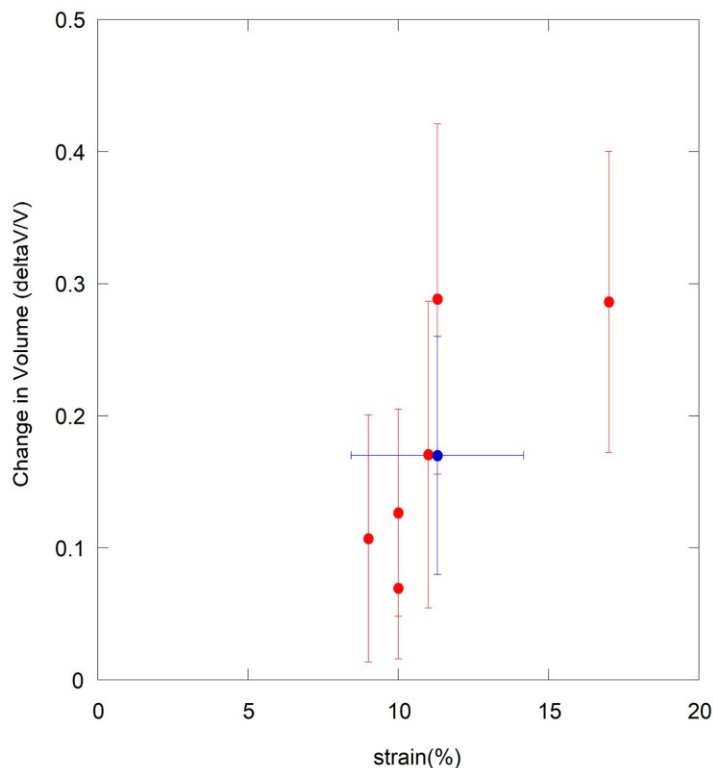


Fig. 3.15: Plot of change in volume vs. weighted average of strain, the blue point represents mean values of change in volume and weighted strain average with standard deviations.

3.7 Energetics involved in molecular denaturation process

For each fibril we were also able to extract the amount of mechanical energy per unit dry volume used to stretch it to its maximum achieved strain by integrating the force versus distance curve.

For this analysis we limit ourselves to the six cases identified in section 3.6.

The energy density vs. strain graph (Fig.3.16A) shows no clear trends, with four fibrils reaching strains between 9 and 17% for an energy density around 7 MJ/m^3 while two other fibrils required

approximately two-fold the energy density, respectively, to reach similar strains. This variation is likely due to the already reported variability in tensile properties of single fibrils extracted from the same tendon type⁶⁹. The percentage change in dry volume after the manipulation was plotted as the function of mechanical energy density used to stretch the fibril to its maximum achieved strain (Fig.3.15B). Again, we have found no clear trends, measurable denaturation occurs for energy densities above 5 MJ/m³. Four fibrils show volume change between 10 and 30 percent in response to a mechanical energy density input between 5 and 10 MJ/m³. 17% volume loss happened for energy density of 11±7 MJ/m³, therefore in average, we might expect that one requires 67±41 MJ/m³ to denature a fibril completely.

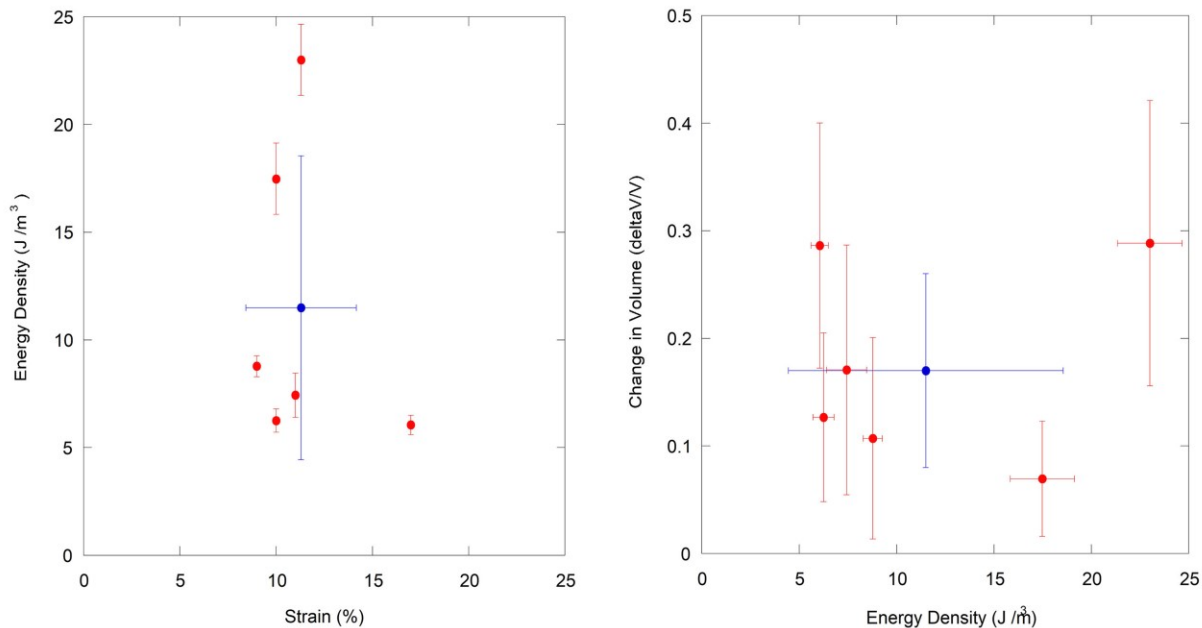


Fig.3.16: (A) Fraction of volume loss after manipulation as function of mechanical energy given to stretch the fibril. (B) The mechanical energy has been plotted against weighted strain average, average values has been shown by blue point with standard deviations.

Chapter 4

Discussion

4.1 Fibril Damage

This stress relaxation experiment on single fibrils showed different level of molecular damage keeping the supramolecular structure intact. The bowstring pulling geometry allowed us to stretch a fibril in such a way that two sides of the same fibril experienced different level of strain. It is evident from Fig 3.6 that fibrils experiencing two different level of strain shows different level of damage, the more strained side of the fibril always experienced more damage in all eight cases. In few cases (Fig 3.6 A,C,E), the fluorescence intensity level roughly doubled or more on the high strain side, however, only six cases showed statistically significant difference. This is the first time demonstration of different strain induced molecular denaturation levels occurring along the same fibril.

The damage contrast between high strain region and low strain region along the same fibril inspired us to investigate the correlation between fluorescence intensity and strain applied in all segments (taking all symmetric and asymmetric cases into consideration). The plot in Fig 3.8 A showed the overall behavior, the more strain leads to more unfolding (all the denaturation we observe after releasing the fibril is due to plastic deformation). The linear fit showed statistically significant trend but did not capture the Physics of the process, which is indicated by Fig. 3.7, rather it seems that there exists two levels of fluorescence intensity. Therefore, I propose to use a sigmoidal fit in order to qualitatively capture this behavior (Fig. 4.1 A). The mean fluorescence intensity increase around 10% strain highlighted by the sigmoidal fit can be understood in term

of the typical stress-strain curve obtained on the same fibrils by Quigley et al.⁵⁵. They observed that after 10% strain positional fibrils extend easily as their stiffness decreases⁵⁵. They proposed that molecular sliding occurs beyond 10% strain thus leading to the observed stiffness reduction⁵⁵. A gradual switch from molecular stretching to molecular sliding would explain the plateau we observe above 10% strain in our mean fluorescence intensity versus strain curve (Fig. 4.1 A).

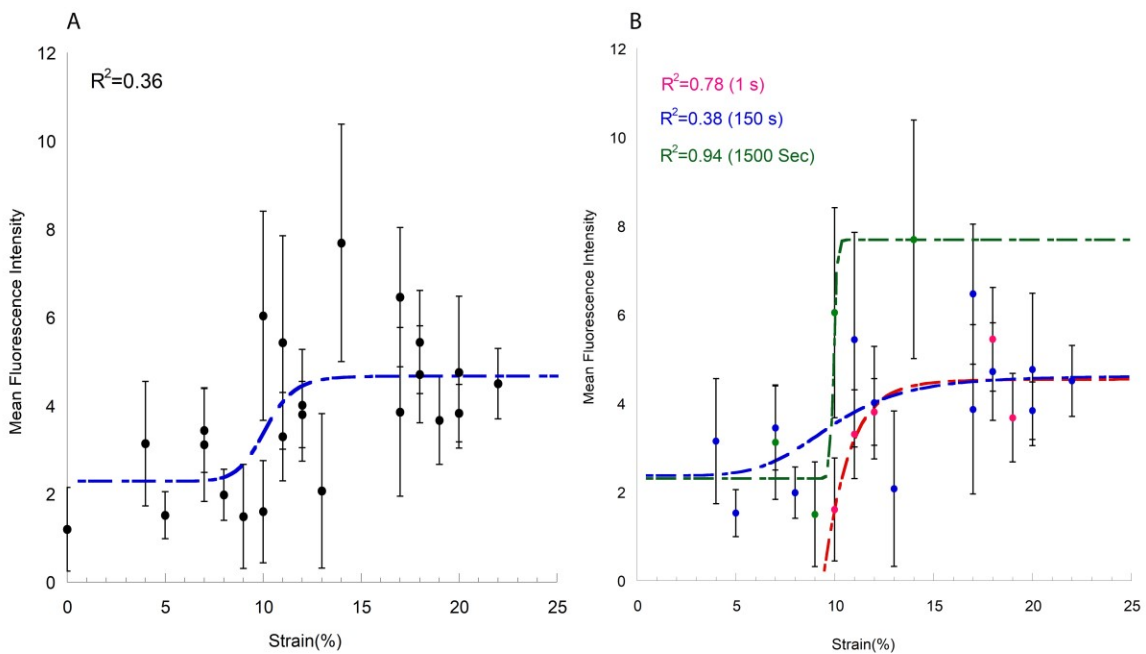


Fig. 4.1: Sigmoidal fitting of mean fluorescence intensity and strain plot for (A) all fibrils and (B) different relaxation time categories

Another interesting feature comes up when we consider each group of relaxation time (Fig. 4.1 B) separately. All three curves follow sigmoidal trend indicating some threshold strain roughly around 10%. Based on the fitting, one can argue that for a given strain above the threshold the longer the stress relaxation the more collagen denaturation occurs.

This claim, however, has two limitations. Firstly, the 1 s and 1500 s cases have few data points compared to 150 s test group. Secondly, the error bars associated with most data points are overlapping one another group. Though we can not make a solid claim, we can hypothesize that during relaxation the molecules stay under tension for a long time which leads to more denaturation. It seems that during the stress relaxation the molecules within the fibril reorganize so that the extent of denaturation that we have observed corresponds to the molecules which have undergone plastic deformation.

4.2 Calibration of Molecular unfolding

For the first time, we have calibrated the number of molecules unfolded in a single collagen fibril from the mean fluorescence intensity observed and the cross-sectional area loss due to manipulation. In an ideal case, if we consider a structurally perfectly homogenous fibril, one could expect that CHP binding would be uniform everywhere along the length of the fibril. Because we had structural variation along the length of the fibril, that enabled us to observe cases where correlation between area loss and fluorescence intensity was found to be linear (Fig.3.13). In our calibration, we have considered that unfolding of a molecule leads to total shrinkage of cross-sectional area, that means cross-sectional area loss was equal to the number of molecules unfolded due to manipulation. This simplified way of calibration is an underestimation of total molecular unfolding since it is possible that some molecules might not get reduced to approximately zero cross-sectional area, they might not shrink much even after unfolding. In our calibration, we have considered shrinkage in cross-sectional area numerically equal to the number of molecular unfolding. Therefore, loss of 1nm^2 of cross-sectional area may correspond

to more than one molecule unfolded or molecular unfolding event. Experimental steps like dehydrating the fibrils or changes in supramolecular structure of fibril might have some impact on the changes we have observed in cross sectional area. We did not have humidity control in experimental set up, therefore, the impact of humidity on fibril morphology was ignored. It might be also possible that even swollen area contained denatured molecules. Therefore, our estimation of molecular unfolding is the lowest limit of molecular unfolding event that took place.

The fluorescence intensity we have observed has been considered as an estimation of CHP binding, but we did not have estimation of how much CHP molecules attached on the fibril surface or how long CHP molecules penetrated inside the fibril.

4.3 The energetics of mechanical denaturation

There have been a number of studies that demonstrated tensile overload leads to molecular level denaturation. Zitnay et al. performed steered molecular dynamics simulation to understand the molecular unfolding process⁷³. One alpha-carbon atom at the N-terminus of one chain of the molecule was fixed and tensile force was applied at the carbon at atom of C-terminal of another chain for stretching with loading speed of $0.002 \text{ \AA ps}^{-1}$ using steered molecular dynamics. The structure was allowed to relax for 40 ns, Visual Molecular Dynamics (VMD) was employed to observe the unfolding mechanisms. Two possible mechanism for molecular loading mechanism was proposed. First, a tension dominant mechanism where it was assumed that the stress is transferred directly from the fibril to molecule, breaking the peptide backbone of one or more α -chains. Second, a shear dominant mechanism where the stress transfer is mediated through cross links that results in intermolecular sliding. As a result of intermolecular sliding, single α -

chain is pulled out from the triple helix (Fig. 4.2 A). Analysis of stress-strain curves obtained from the molecular dynamics simulation showed that the shear-dominant mechanism leads to irreversible failure around 13% strain with a maximum applied force around 600 pN peak force while the tension dominant case does not show any sign of irreversible failure even at 20% strain and 3,000 pN force. Therefore, the likely mechanism of molecular level failure was proposed as shear dominant, compatible with experimental observations. Simulation snapshots and a measurement of triple helix unfolding known as Solvent accessible surface area (SASA) also indicated that shear dominant loading mechanism leads to molecular unfolding (Fig. 4.2 C & D) around 13% strain. For comparing our experimental result with the result explained above, we have computed the energy required for unfolding a single triple helix from Fig. 4.2 C. The strain was converted into length, hence integrating the Force-length curve up to around 13% strain, we calculated the mechanical energy density necessary to unfold the molecule to be around 30 MJ/m³. This energy is in agreement with the lower bound of our estimated range 26-108 MJ/m³ (Fig. 3.16 B). In addition, Herod et al. demonstrated using DSC that the energy required to thermally denatured fibrils in CDE tendons is 130±31 MJ/m³ and is compatible with our upper bound for mechanical denaturation.

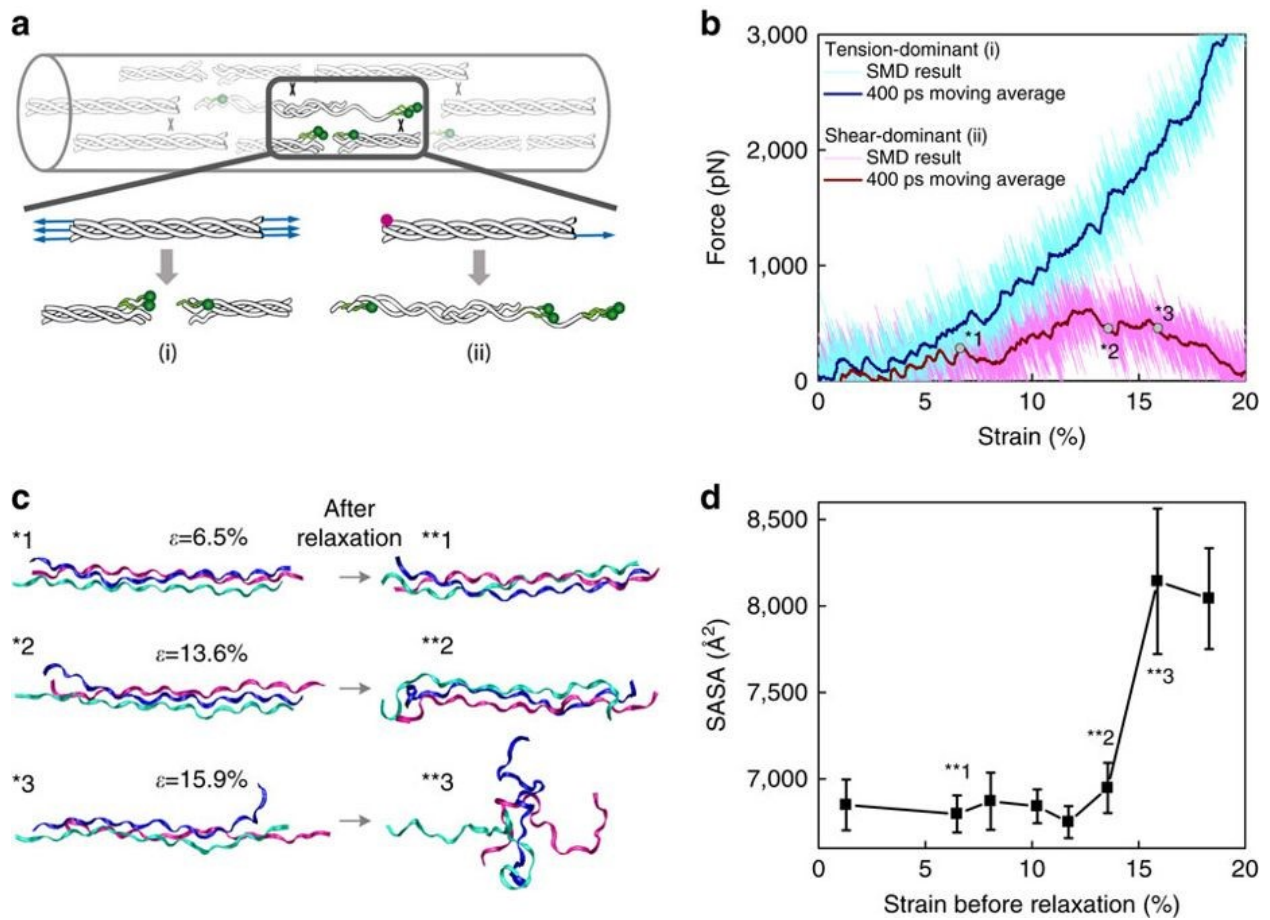


Fig. 4.2: (a) Two loading mechanisms that were proposed through simulations: the tension-dominant (i) and the shear-dominant case (ii). (b) Force-strain curves for tension and shear dominant loading case (c) Simulation snapshots for the shear-dominant case, unfolding was detected around 13% strain (d) SASA measurement of triple helix, structural changes started at 13.6% strain. Figure adapted from⁷³

There have been few works related to evidence of mechanical unfolding in tendon and molecular level that indicated effect of strain rate^{67,93}. With the aid of steered molecular dynamics a collagen peptide sequence $[(\text{Gly-Pro-Hyp})_{10}]_3$ was stretched with pulling rate in the range from

0.01 to 100 m/s, it has been observed that slower strain made more unfolding because it gives time to system to respond⁹³. A similar phenomena, strain rate dependence in mechanical unloading has been investigated by Willet et al. where lower strain rate leads more denaturation⁶⁷. In our study, we did not have a constant strain rate, and the maximum strain rate for each fibril varied widely from 3 to 11%/s with an average around 6%/s

4.4 Comparison with Rupture Mechanics

Quigley et al. developed the bowstring geometry which has been used in this study to stretch the fibrils⁵⁵. They have stretched single collagen fibrils extracted from bovine CDET and SDFT up to rupture strain in order to study the rupture mechanics and morphological features of the damaged fibrils. The study showed that the collagen fibrils extracted from functionally different tissue respond mechanically in different ways. Though I investigated only the CDET fibrils, the same pulling technique and partially similar experimental protocol warrant a comparison between the two studies. In my study, I stretched CDET single fibrils at different strain, held them for different relaxation time – the motive of the study was not to rupture single fibrils.

The first structural feature Quigley et al. observed in ruptured CDET fibrils is the formation of repeating kinks along their length which were due to the disruption of their inner core, the kinks appeared at discrete locations along the length of the fibril, separated by intact D-banding region. Shell delamination was the second major structural feature in post-rupture CDET fibril morphology. The significant disruption of the fibril surface created a loose layer or shell, lacking D-banding. Therefore, significant molecular level disorder happened at the fibril surface. In our case, no such serial kinking or shell delamination was observed, post manipulated AFM image

analysis showed around 17% volume loss with almost no change in D-band, that is, the molecular packing in the fibril was not disturbed that much while 17% of all the triple helices permanently denatured yielding to the overall volume shrinkage. Quigley et al. reported approximately 44% loss of materials from the fibril periphery as shell delamination occurred. Quigley et al. also reported toughness of CDET fibrils, $45 \pm 15 \text{ MJ/m}^3$ which represents the mechanical energy density the fibril can absorb before rupturing, the mean energy our fibrils absorbed during stretching is around 11 MJ/m^3 , four times smaller energy than the toughness of CDET fibrils.

Fig. 4.3 is the reconstruction of Volume-Strain plot of Fig. 3.15. In this plot we have added an additional blue data point, which represents the change in volume measured after rupture⁵⁵. The observed behavior is in agreement with the sigmoidal fit used in Fig. 4.1, even so we do not have any data point below 9% strain. Most of the molecular denaturation occurs around 10% strain and increases moderately after that. However, it is likely that our calibration method overestimates the molecular damage accrued by the fibrils in our experiment. Otherwise it would be difficult to reconcile the fact that at 17% strain we observe around 30% denaturation in volume without the appearance of a denatured shell whereas ruptured fibrils reached 40% denaturation in volume and had a noticeable shell layer⁵⁵.

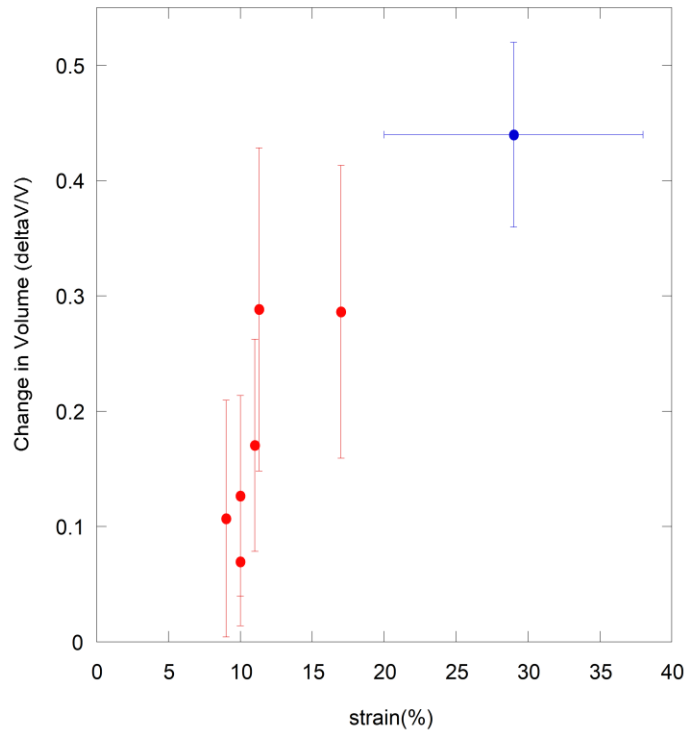


Fig. 4.3: Non linear response of the collagen molecular denaturation as a function strain. The blue data point represents rupture strain and corresponding volume change obtained by Quigley et al.⁵⁵

4.5 Physiological Significance

The most important physiological aspect of this research is detection of permanent molecular level damage in single fibril without rupture. While previous studies focused on damage at the fibril level^{69,94,95}, molecular level damage was acknowledged only in case of highly damaged tissues^{25,67}. Our data implies that irreversible molecular level damage is detectable even at low strain or subfailure loading at single fibril level. Zitnay et al. also experimentally observed such irreversible molecular damage in tendon level investigation which indicated that molecular level damage plays crucial role in tendon damage during subfailure loading⁷³.

Under different physiological conditions, tendons can receive enough strain due to strenuous exercise which is related to tendinopathies⁹⁶. It has been suggested earlier that the fibril level receives 30% of the total strain applied at the tendon level⁹⁷. The rupture strain of the CDET has been previously reported above 50% strain, this corresponds to above 15% strain achieved at the fibril level⁵⁴ but earlier studies suggested that even subfailure loading can lead to damage in connective tissues⁹⁷⁻⁹⁹. Therefore, subfailure level damage in tendon might induce low but enough strain in fibril level which can lead to molecular unfolding. Mechanical damage or subfailure tissue damage is observed in clinically debilitating condition like tendinosis which results from overuse or repeated subfailure loading^{100,101}. Therefore, understanding the nature and evolution of damage from molecular level is important for clinical applications.

Chapter 5

Conclusion

This study has several important outcomes. Firstly, this study demonstrated for the first time that the mechanical denaturation of CDET collagen fibrils might happen at low strain, in a non-disruptive test, keeping the supramolecular structure intact. The fluorescence intensity level varied in even same fibril that experienced two different strain levels in asymmetric bowstring geometry. Secondly, the CHP binding increased significantly with strain – medium and high strain level led to more unfolding than the low strain. The fluorescence intensity seems to follow a sigmoidal trend when it is plotted against the strain applied, a trend that was also observed at the tendon level. The effect of different relaxation times in molecular unfolding was investigated as well. Thirdly, quantitative analysis was done on post-manipulated fibril morphology. The area loss due to molecular denaturation has been quantified and has been plotted against the fluorescence intensity observed which showed significant linear trend in six cases. Then the fraction of volume loss in non-ruptured fibrils has been quantified and was explained as a function of strain applied. Lastly, mechanical energy for molecular unfolding a single fibril was computed for the first time, plotted against the strain and fraction of volume loss to understand the energetics and associated morphological changes that took place after stress relaxation. While the other stress relaxation studies did not make any conclusive remarks about fibril morphology after stress relaxation, this study can be helpful for further investigation. Also the structural changes we have observed through a non-disruptive test can be inspiring for understanding the damage mechanism in more details in the future.

Next Steps:

(i) This study has only used one tendon type, therefore, the effect of variation in cross-link in two different tendon types has not been investigated. It has been seen that collagen fibrils from functionally different tendon have different mechanical response, hence, two different types of tendon can be used as sample.

(ii) The fibrils have been pulled up to a certain strain, held and then released. The effect of fast release after relaxation was not investigated in this study, therefore, it would be interesting to see the effect of controlled release.

(iii) What is the effect of different pulling speed without rupturing the fibrils? The same relaxation experiment can be performed with different strain rates.

(iv) In this study, the highest targeted strain was 20%. It would be interesting to pull some fibrils with near rupture strain to see whether longer relaxation time can induce shell delamination or kink appearance.

(v) In order to understand the role of cross-links, cross-linkers can be introduced in some fibrils. This would allow to compare post manipulated morphological features of native and cross-linked fibrils.

References

1. Veis A. Collagen fibrillar structure in mineralized and nonmineralized tissues. *Curr Opin Solid State Mater Sci.* 1997. doi:10.1016/S1359-0286(97)80130-1
2. Ricard-Blum S. The Collagen Family. *Cold Spring Harb Perspect Biol.* 2011. doi:10.1101/cshperspect.a004978
3. Canty EG. Procollagen trafficking, processing and fibrillogenesis. *J Cell Sci.* 2005. doi:10.1242/jcs.01731
4. Svensson RB, Hassenkam T, Hansen P, Kjaer M, Magnusson SP. Tensile force transmission in human patellar tendon fascicles is not mediated by glycosaminoglycans. *Connect Tissue Res.* 2011. doi:10.3109/03008207.2010.551569
5. Screen HRC, Shelton JC, Chhaya VH, Kayser M V., Bader DL, Lee DA. The influence of noncollagenous matrix components on the micromechanical environment of tendon fascicles. *Ann Biomed Eng.* 2005. doi:10.1007/s10439-005-5777-9
6. Bozec L, Van Der Heijden G, Horton M. Collagen fibrils: Nanoscale ropes. *Biophys J.* 2007. doi:10.1529/biophysj.106.085704
7. Silver FH, Freeman JW, Seehra GP. Collagen self-assembly and the development of tendon mechanical properties. *J Biomech.* 2003. doi:10.1016/S0021-9290(03)00135-0
8. Cowan PM, McGavin S, North ACT. The polypeptide chain configuration of collagen. *Nature.* 1955. doi:10.1038/1761062a0
9. Rich A, Crick FHC. The molecular structure of collagen. *J Mol Biol.* 1961. doi:10.1016/S0022-2836(61)80016-8
10. van der Rest M, Garrone R. Collagen family of proteins. *FASEB J.* 1991.

doi:10.1096/fasebj.5.13.1916105

11. Kramer RZ, Bella J, Brodsky B, Berman HM. The crystal and molecular, structure of a collagen-like peptide with a biologically relevant sequence. *J Mol Biol.* 2001.
doi:10.1006/jmbi.2001.4849
12. Beck K, Brodsky B. Supercoiled protein motifs: The collagen triple-helix and the α - helical coiled coil. *J Struct Biol.* 1998. doi:10.1006/jsbi.1998.3965
13. Ottani V, Martini D, Franchi M, Ruggeri A, Raspanti M. Hierarchical structures in fibrillar collagens. *Micron.* 2002. doi:10.1016/S0968-4328(02)00033-1
14. Kalson NS, Lu Y, Taylor SH, Holmes DF, Kadler KE. A structure-based extracellular matrix expansion mechanism of fibrous tissue growth. *Elife.* 2015. doi:10.7554/eLife.05958
15. Hodge AJ, Petruska JA. Recent studies with the electron microscope on ordered aggregates of the tropocollagen macromolecule. In: *Aspects of Protein Structure.* ; 1963.
16. Orgel JPRO, Irving TC, Miller A, Wess TJ. Microfibrillar structure of type I collagen in situ. *Proc Natl Acad Sci.* 2006. doi:10.1073/pnas.0502718103
17. Schmitt FO, Hall CE, Jakus MA. Electron microscope investigations of the structure of collagen. *J Cell Comp Physiol.* 20(1):11-33. doi:10.1002/jcp.1030200103
18. Gathercole LJ, Miles MJ, McMaster TJ, Holmes DF. Scanning probe microscopy of collagen I and pN-collagen I assemblies and the relevance to scanning tunnelling microscopy contrast generation in proteins. *J Chem Soc Faraday Trans.* 1993.
doi:10.1039/FT9938902589
19. Chernoff EAG, Chernoff DA. Atomic force microscope images of collagen fibers. *J Vac Sci Technol A.* 1992;10(4):596-599. doi:10.1116/1.577736

20. Eyre DR, Wu J-J. Collagen Cross-Links. In: Brinckmann J, Notbohm H, Müller PK, eds. *Collagen: Primer in Structure, Processing and Assembly*. Berlin, Heidelberg: Springer Berlin Heidelberg; 2005:207-229. doi:10.1007/b103828
21. Bailey AJ, Paul RG, Knott L. Mechanisms of maturation and ageing of collagen. *Mech Ageing Dev*. 1998. doi:10.1016/S0047-6374(98)00119-5
22. Miles CA, Ghelashvili M. Polymer-in-a-box mechanism for the thermal stabilization of collagen molecules in fibers. *Biophys J*. 1999. doi:10.1016/S0006-3495(99)77476-X
23. Miles CA, Avery NC, Rodin V V., Bailey AJ. The increase in denaturation temperature following cross-linking of collagen is caused by dehydration of the fibres. *J Mol Biol*. 2005. doi:10.1016/j.jmb.2004.12.001
24. BATSON EL, PARAMOUR RJ, SMITH TJ, BIRCH HL, PATTERSON-KANE JC, GOODSHIP AE. Are the material properties and matrix composition of equine flexor and extensor tendons determined by their functions? *Equine Vet J*. 2010. doi:10.2746/042516403776148327
25. Willett TL, Labow RS, Lee JM. Mechanical overload decreases the thermal stability of collagen in an in vitro tensile overload tendon model. *J Orthop Res*. 2008. doi:10.1002/jor.20672
26. Rumian AP, Wallace AL, Birch HL. Tendons and Ligaments Are Anatomically Distinct But Overlap in Molecular and Morphological Features—A Comparative Study in an Ovine Model. *J Orthop Res*. 2007. doi:10.1002/jor.20218
27. Amiel D, Frank C, Harwood F, Fronck J, Akeson W. Tendons and ligaments: A morphological and biochemical comparison. *J Orthop Res*. 1983.

doi:10.1002/jor.1100010305

28. Canty EG, Kadler KE. Collagen fibril biosynthesis in tendon: A review and recent insights. In: *Comparative Biochemistry and Physiology - A Molecular and Integrative Physiology.* ; 2002. doi:10.1016/S1095-6433(02)00212-X
29. Keene DR, Sakai LY, Bachinger HP, Burgerson RE. Type III collagen can be present on banded collagen fibrils regardless of fibril diameter. *J Cell Biol.* 1987. doi:10.1083/jcb.105.5.2393
30. Zeugolis DI, Li B, Lareu RR, Chan CK, Raghunath M. Collagen solubility testing, a quality assurance step for reproducible electro-spun nano-fibre fabrication. A technical note. *J Biomater Sci Polym Ed.* 2008. doi:10.1163/156856208786052344
31. Zeugolis DI, Paul RG, Attenburrow G. Factors influencing the properties of reconstituted collagen fibers prior to self-assembly: Animal species and collagen extraction method. *J Biomed Mater Res - Part A.* 2008. doi:10.1002/jbm.a.31694
32. Fan L, Sarkar K, Franks DJ, Uthoff HK. Estimation of total collagen and types I and III collagen in canine rotator cuff tendons. *Calcif Tissue Int.* 1997. doi:10.1007/s002239900327
33. Koob TJ, Vogel KG. Site-related variations in glycosaminoglycan content and swelling properties of bovine flexor tendon. *J Orthop Res.* 1987. doi:10.1002/jor.1100050314
34. Kirkendall DT, Garrett WE. Function and biomechanics of tendons. *Scand J Med Sci Sports.* 2007. doi:10.1111/j.1600-0838.1997.tb00120.x
35. Fessel G, Snedeker JG. Evidence against proteoglycan mediated collagen fibril load transmission and dynamic viscoelasticity in tendon. *Matrix Biol.* 2009.

doi:10.1016/j.matbio.2009.08.002

36. Kjellen L, Lindahl U. Proteoglycans: structures and interactions. *Annu Rev Biochem.* 1991;60:443-475. doi:10.1146/annurev.bi.60.070191.002303
37. Yoon JH, Halper J. Tendon proteoglycans: biochemistry and function. *J Musculoskelet Neuronal Interact.* 2005;5(1):22-34.
38. Scott JE, Orford CR, Hughes EW. Proteoglycan-collagen arrangements in developing rat tail tendon: an electron microscopical and biochemical investigation. *Biochem J.* 1981. doi:10.1042/bj1950573
39. Elliott D. Structure and function of mammalian tendon. *Biol Rev.* 1965. doi:10.1111/j.1469-185X.1965.tb00808.x
40. Scott JE. Extracellular matrix, supramolecular organisation and shape. *J Anat.* 1995.
41. Torp S, Baer E, Friedman B. Effects of age and of mechanical deformation on the ultrastructure of tendon. *Struct Fibrous Biopolym.* 1975;26:223-250.
42. Grant TM, Yapp C, Chen Q, Czernuszka JT, Thompson MS. The Mechanical, Structural, and Compositional Changes of Tendon Exposed to Elastase. *Ann Biomed Eng.* 2015. doi:10.1007/s10439-015-1308-5
43. Kastelic J, Baer E. Deformation in tendon collagen. *Symp Soc Exp Biol.* 1980;34:397-435.
44. Veres SP, Harrison JM, Lee JM. Repeated subrupture overload causes progression of nanoscaled discrete plasticity damage in tendon collagen fibrils. *J Orthop Res.* 2013. doi:10.1002/jor.22292
45. Fratzl P, Misof K, Zizak I, Rapp G, Amenitsch H, Bernstorff S. Fibrillar structure and mechanical properties of collagen. *J Struct Biol.* 1998. doi:10.1006/jsbi.1998.3966

46. Diamant J, Keller A, Baer E, Litt M, Arridge RGC. Collagen; Ultrastructure and Its Relation to Mechanical Properties as a Function of Ageing. *Proc R Soc B Biol Sci.* 1972.
doi:10.1098/rspb.1972.0019
47. Folkhard W, Mosler E, Geercken W, et al. Quantitative analysis of the molecular sliding mechanisms in native tendon collagen - time-resolved dynamic studies using synchrotron radiation. *Int J Biol Macromol.* 1987. doi:10.1016/0141-8130(87)90047-X
48. Alexander R. Elastic Energy Stores in Running Vertebrates. *Am Zool.* 1984.
49. Alexander RMN, Vernon A. The mechanics of hopping by kangaroos (Macropodidae). *J Zool.* 1975. doi:10.1111/j.1469-7998.1975.tb05983.x
50. Birch HL. Tendon matrix composition and turnover in relation to functional requirements. In: *International Journal of Experimental Pathology.* ; 2007.
doi:10.1111/j.1365-2613.2007.00552.x
51. Thorpe CT, Klemm C, Riley GP, Birch HL, Clegg PD, Screen HRC. Helical sub-structures in energy-storing tendons provide a possible mechanism for efficient energy storage and return. *Acta Biomater.* 2013. doi:10.1016/j.actbio.2013.05.004
52. Thorpe CT, Udeze CP, Birch HL, Clegg PD, Screen HRC. Specialization of tendon mechanical properties results from interfascicular differences. *J R Soc Interface.* 2012.
doi:10.1098/rsif.2012.0362
53. KER RF, ALEXANDER RM, BENNETT MB. Why are mammalian tendons so thick? *J Zool.* 1988. doi:10.1111/j.1469-7998.1988.tb02432.x
54. Herod TW, Chambers NC, Veres SP. Collagen fibrils in functionally distinct tendons have differing structural responses to tendon rupture and fatigue loading. *Acta Biomater.*

2016. doi:10.1016/j.actbio.2016.06.017
55. Quigley AS, Bancelin S, Deska-Gauthier D, Légaré F, Kreplak L, Veres SP. In tendons, differing physiological requirements lead to functionally distinct nanostructures. *Sci Rep*. 2018. doi:10.1038/s41598-018-22741-8
56. Quigley AS, Veres SP, Kreplak L. Bowstring stretching and quantitative imaging of single collagen fibrils via atomic force microscopy. *PLoS One*. 2016. doi:10.1371/journal.pone.0161951
57. Svensson RB, Mulder H, Kovanen V, Magnusson SP. Fracture mechanics of collagen fibrils: Influence of natural cross-links. *Biophys J*. 2013. doi:10.1016/j.bpj.2013.04.033
58. Uzel SGM, Buehler MJ. Molecular structure, mechanical behavior and failure mechanism of the C-terminal cross-link domain in type I collagen. *J Mech Behav Biomed Mater*. 2011. doi:10.1016/j.jmbbm.2010.07.003
59. Dittmore A, Silver J, Sarkar SK, Marmer B, Goldberg GI, Neuman KC. Internal strain drives spontaneous periodic buckling in collagen and regulates remodeling. *Proc Natl Acad Sci*. 2016. doi:10.1073/pnas.1523228113
60. Teng X, Hwang W. Chain registry and load-dependent conformational dynamics of collagen. *Biomacromolecules*. 2014. doi:10.1021/bm500641f
61. Fields GB. A model for interstitial collagen catabolism by mammalian collagenases. *J Theor Biol*. 1991. doi:10.1016/S0022-5193(05)80157-2
62. Stultz CM. Localized unfolding of collagen explains collagenase cleavage near imino-poor sites. *J Mol Biol*. 2002. doi:10.1016/S0022-2836(02)00421-7
63. Adhikari AS, Chai J, Dunn AR. Mechanical load induces a 100-fold increase in the rate of

- collagen proteolysis by MMP-1. *J Am Chem Soc.* 2011. doi:10.1021/ja109972p
64. Miles CA, Bailey AJ. Thermal denaturation of collagen revisited. *Proc Indian Acad Sci.* 1999. doi:10.1007/BF02869897
 65. Fraser RDB, MacRae TP, Suzuki E. Chain conformation in the collagen molecule. *J Mol Biol.* 1979. doi:10.1016/0022-2836(79)90507-2
 66. Kwansa AL, De Vita R, Freeman JW. Mechanical recruitment of N- and C-crosslinks in collagen type I. *Matrix Biol.* 2014. doi:10.1016/j.matbio.2013.10.012
 67. Willett TL, Labow RS, Avery NC, Lee JM. Increased proteolysis of collagen in an in vitro tensile overload tendon model. *Ann Biomed Eng.* 2007;35(11):1961-1972. doi:10.1007/s10439-007-9375-x
 68. Veres SP, Harrison JM, Lee JM. Mechanically overloading collagen fibrils uncoils collagen molecules, placing them in a stable, denatured state. *Matrix Biol.* 2014. doi:10.1016/j.matbio.2013.07.003
 69. Veres SP, Lee JM. Designed to fail: A novel mode of collagen fibril disruption and its relevance to tissue toughness. *Biophys J.* 2012. doi:10.1016/j.bpj.2012.05.022
 70. Li Y, Foss CA, Summerfield DD, et al. Targeting collagen strands by photo-triggered triple-helix hybridization. *Proc Natl Acad Sci.* 2012. doi:10.1073/pnas.1209721109
 71. Li Y, Yu SM. Targeting and mimicking collagens via triple helical peptide assembly. *Curr Opin Chem Biol.* 2013. doi:10.1016/j.cbpa.2013.10.018
 72. Li Y, Ho D, Meng H, et al. Direct detection of collagenous proteins by fluorescently labeled collagen mimetic peptides. *Bioconjug Chem.* 2013. doi:10.1021/bc3005842
 73. Zitnay JL, Li Y, Qin Z, et al. Molecular level detection and localization of mechanical

- damage in collagen enabled by collagen hybridizing peptides. *Nat Commun.* 2017.
doi:10.1038/ncomms14913
74. Svensson RB, Hassenkam T, Hansen P, Peter Magnusson S. Viscoelastic behavior of discrete human collagen fibrils. *J Mech Behav Biomed Mater.* 2010.
doi:10.1016/j.jmbbm.2009.01.005
75. Svensson RB, Hassenkam T, Grant CA, Magnusson SP. Tensile properties of human collagen fibrils and fascicles are insensitive to environmental salts. *Biophys J.* 2010.
doi:10.1016/j.bpj.2010.11.018
76. Svensson RB, Hansen P, Hassenkam T, et al. Mechanical properties of human patellar tendon at the hierarchical levels of tendon and fibril. *J Appl Physiol.* 2012.
doi:10.1152/jappphysiol.01172.2011
77. Yang L, van der Werf KO, Dijkstra PJ, Feijen J, Bennink ML. Micromechanical analysis of native and cross-linked collagen type I fibrils supports the existence of microfibrils. *J Mech Behav Biomed Mater.* 2012;6:148-158. doi:10.1016/j.jmbbm.2011.11.008
78. Graham JS, Vomund AN, Phillips CL, Grandbois M. Structural changes in human type I collagen fibrils investigated by force spectroscopy. *Exp Cell Res.* 2004.
doi:10.1016/j.yexcr.2004.05.022
79. Van Der Rijt JAJ, Van Der Werf KO, Bennink ML, Dijkstra PJ, Feijen J. Micromechanical testing of individual collagen fibrils. *Macromol Biosci.* 2006.
doi:10.1002/mabi.200600063
80. Shen ZL, Dodge MR, Kahn H, Ballarini R, Eppell SJ. Stress-strain experiments on individual collagen fibrils. *Biophys J.* 2008. doi:10.1529/biophysj.107.124602

81. Eppell SJ, Smith BN, Kahn H, Ballarini R. Nano measurements with micro-devices: Mechanical properties of hydrated collagen fibrils. *J R Soc Interface*. 2006. doi:10.1098/rsif.2005.0100
82. Shen ZL, Kahn H, Ballarini R, Eppell SJ. Viscoelastic Properties of Isolated Collagen Fibrils. *Biophys J*. 2011;100(12):3008-3015. doi:10.1016/j.bpj.2011.04.052
83. Sader JE. frequency response of cantilever beams immersed in viscous fluids with applications to the atomic force microscope. *J Appl Phys*. 1998. doi:10.1063/1.368002
84. Gnecco E, Bennewitz R, Socoliuc A, Meyer E. Friction and wear on the atomic scale. *Wear*. 2003. doi:10.1016/S0043-1648(03)00236-9
85. Green CP, Lioe H, Cleveland JP, Proksch R, Mulvaney P, Sader JE. Normal and torsional spring constants of atomic force microscope cantilevers. *Rev Sci Instrum*. 2004. doi:10.1063/1.1753100
86. Hess P. Laser diagnostics of mechanical and elastic properties of silicon and carbon films. *Appl Surf Sci*. 1996. doi:10.1016/S0169-4332(96)00369-8
87. Fields GB. Synthesis and biological applications of collagen-model triple-helical peptides. *Org Biomol Chem*. 2010. doi:10.1039/b920670a
88. Bozec L, Odlyha M. Thermal denaturation studies of collagen by microthermal analysis and atomic force microscopy. *Biophys J*. 2011. doi:10.1016/j.bpj.2011.04.033
89. Lin S-J, Lo W, Tan H-Y, et al. Prediction of heat-induced collagen shrinkage by use of second harmonic generation microscopy. *J Biomed Opt*. 2006. doi:10.1117/1.2209959
90. Uhlig MR, Magerle R. Unraveling capillary interaction and viscoelastic response in atomic force microscopy of hydrated collagen fibrils. *Nanoscale*. 2017. doi:10.1039/c6nr07697a

91. Isobe T, Feigelson ED, Akritas MG, Babu GJ. Linear regression in astronomy. *Astrophys J*. 1990. doi:10.1086/169390
92. Hulmes DJ, Wess TJ, Prockop DJ, Fratzl P. Radial packing, order, and disorder in collagen fibrils. *Biophys J*. 1995. doi:10.1016/S0006-3495(95)80391-7
93. Gautieri A, Buehler MJ, Redaelli A. Deformation rate controls elasticity and unfolding pathway of single tropocollagen molecules. *J Mech Behav Biomed Mater*. 2009. doi:10.1016/j.jmbbm.2008.03.001
94. Shepherd JH, Riley GP, Screen HRC. Early stage fatigue damage occurs in bovine tendon fascicles in the absence of changes in mechanics at either the gross or micro-structural level. *J Mech Behav Biomed Mater*. 2014. doi:10.1016/j.jmbbm.2014.06.005
95. Fung DT, Wang VM, Laudier DM, et al. Subrupture tendon fatigue damage. *J Orthop Res*. 2009. doi:10.1002/jor.20722
96. Hreljac A, Marshall RN, Hume PA. Evaluation of lower extremity overuse injury potential in runners. *Med Sci Sports Exerc*. 2000. doi:10.1097/00005768-200009000-00018
97. Puxkandl R, Zizak I, Paris O, et al. Viscoelastic properties of collagen: synchrotron radiation investigations and structural model. *Philos Trans R Soc Lond B Biol Sci*. 2002. doi:10.1098/rstb.2001.1033
98. Cheng VWT, Screen HRC. The micro-structural strain response of tendon. *J Mater Sci*. 2007. doi:10.1007/s10853-007-1653-3
99. Fung DT, Wang VM, Andarawis-Puri N, et al. Early response to tendon fatigue damage accumulation in a novel in vivo model. *J Biomech*. 2010. doi:10.1016/j.jbiomech.2009.08.039

100. Kraushaar BS, Nirschl RP. Tendinosis of the elbow (Tennis elbow): Clinical features and findings of histological, immunohistochemical, and electron microscopy studies. *J Bone Jt Surg - Ser A*. 1999. doi:10.2106/00004623-199902000-00014
101. Leadbetter WB. Cell-matrix response in tendon injury. *Clin Sport Med*. 1992.

Appendix

9/5/2018

Rightslink® by Copyright Clearance Center



RightsLink®



Title: Collagen self-assembly and the development of tendon mechanical properties
Author: Frederick H. Silver, Joseph W. Freeman, Gurinder P. Seehra
Publication: Journal of Biomechanics
Publisher: Elsevier
Date: October 2003
Copyright © 2003 Elsevier Science Ltd. All rights reserved.

Logged in as:
S M Asif Iqbal
Dalhousie University
Account #:
3001331337

[LOGOUT](#)

Order Completed

Thank you for your order.

This Agreement between Dalhousie University -- S M Asif Iqbal ("You") and Elsevier ("Elsevier") consists of your license details and the terms and conditions provided by Elsevier and Copyright Clearance Center.

Your confirmation email will contain your order number for future reference.

[printable details](#)

License Number	4422611178342
License date	Sep 05, 2018
Licensed Content Publisher	Elsevier
Licensed Content Publication	Journal of Biomechanics
Licensed Content Title	Collagen self-assembly and the development of tendon mechanical properties
Licensed Content Author	Frederick H. Silver, Joseph W. Freeman, Gurinder P. Seehra
Licensed Content Date	Oct 1, 2003
Licensed Content Volume	36
Licensed Content Issue	10
Licensed Content Pages	25
Type of Use	reuse in a thesis/dissertation
Portion	figures/tables/illustrations
Number of figures/tables/illustrations	1
Format	both print and electronic
Are you the author of this Elsevier article?	No
Will you be translating?	No
Original figure numbers	Fig. 3.
Title of your thesis/dissertation	'STRUCTURAL CHANGES IN STRETCHED COLLAGEN FIBRILS AS A FUNCTION OF RELAXATION TIMES'
Expected completion date	Sep 2018
Estimated size (number of pages)	80
Requestor Location	Dalhousie University 6299 South Street



RightsLink®

[Home](#)
[Account Info](#)
[Help](#)


Title: Fibrillar Structure and Mechanical Properties of Collagen

Author: Peter Fratzl, Klaus Misof, Ivo Zizak, Gert Rapp, Heinz Amenitsch, Sigrid Bernstorff

Publication: Journal of Structural Biology

Publisher: Elsevier

Date: 1998

Logged in as:
S M Asif Iqbal
Dalhousie University
Account #:
3001331337

[LOGOUT](#)

Copyright © 1998 Academic Press. All rights reserved.

Order Completed

Thank you for your order.

This Agreement between Dalhousie University -- S M Asif Iqbal ("You") and Elsevier ("Elsevier") consists of your license details and the terms and conditions provided by Elsevier and Copyright Clearance Center.

Your confirmation email will contain your order number for future reference.

[printable details](#)

License Number	4422620139273
License date	Sep 05, 2018
Licensed Content Publisher	Elsevier
Licensed Content Publication	Journal of Structural Biology
Licensed Content Title	Fibrillar Structure and Mechanical Properties of Collagen
Licensed Content Author	Peter Fratzl, Klaus Misof, Ivo Zizak, Gert Rapp, Heinz Amenitsch, Sigrid Bernstorff
Licensed Content Date	Jan 1, 1998
Licensed Content Volume	122
Licensed Content Issue	1-2
Licensed Content Pages	4
Type of Use	reuse in a thesis/dissertation
Portion	figures/tables/illustrations
Number of figures/tables/illustrations	1
Format	both print and electronic
Are you the author of this Elsevier article?	No
Will you be translating?	No
Original figure numbers	FIG. 1.
Title of your thesis/dissertation	'STRUCTURAL CHANGES IN STRETCHED COLLAGEN FIBRILS AS A FUNCTION OF RELAXATION TIMES'
Expected completion date	Sep 2018
Estimated size (number of pages)	80
Requestor Location	Dalhousie University 6299 South Street



RightsLink®

[Home](#)
[Account Info](#)
[Help](#)


Title: Micromechanical analysis of native and cross-linked collagen type I fibrils supports the existence of microfibrils

Author: L. Yang, K.O. van der Werf, P.J. Dijkstra, J. Feijen, M.L. Bennink

Publication: Journal of the Mechanical Behavior of Biomedical Materials

Publisher: Elsevier

Date: February 2012

Copyright © 2011 Elsevier Ltd. All rights reserved.

Logged in as:
S M Asif Iqbal
Dalhousie University
Account #:
3001331337

[LOGOUT](#)

Order Completed

Thank you for your order.

This Agreement between Dalhousie University -- S M Asif Iqbal ("You") and Elsevier ("Elsevier") consists of your license details and the terms and conditions provided by Elsevier and Copyright Clearance Center.

Your confirmation email will contain your order number for future reference.

[printable details](#)

License Number	4422630430756
License date	Sep 05, 2018
Licensed Content Publisher	Elsevier
Licensed Content Publication	Journal of the Mechanical Behavior of Biomedical Materials
Licensed Content Title	Micromechanical analysis of native and cross-linked collagen type I fibrils supports the existence of microfibrils
Licensed Content Author	L. Yang, K.O. van der Werf, P.J. Dijkstra, J. Feijen, M.L. Bennink
Licensed Content Date	Feb 1, 2012
Licensed Content Volume	6
Licensed Content Issue	n/a
Licensed Content Pages	11
Type of Use	reuse in a thesis/dissertation
Portion	figures/tables/illustrations
Number of figures/tables/illustrations	1
Format	both print and electronic
Are you the author of this Elsevier article?	No
Will you be translating?	No
Original figure numbers	Fig. 2.
Title of your thesis/dissertation	'STRUCTURAL CHANGES IN STRETCHED COLLAGEN FIBRILS AS A FUNCTION OF RELAXATION TIMES'
Expected completion date	Sep 2018
Estimated size (number of pages)	80
Requestor Location	Dalhousie University



RightsLink®

[Home](#)
[Account Info](#)
[Help](#)


Title: Viscoelastic Properties of Isolated Collagen Fibrils

Author: Zhilei Liu Shen, Harold Kahn, Roberto Ballarini, Steven J. Eppell

Publication: Biophysical Journal

Publisher: Elsevier

Date: 22 June 2011

Logged in as:
S M Asif Iqbal
Dalhousie University
Account #:
3001331337

[LOGOUT](#)

Copyright © 2011 Biophysical Society. Published by Elsevier Inc. All rights reserved.

Order Completed

Thank you for your order.

This Agreement between Dalhousie University -- S M Asif Iqbal ("You") and Elsevier ("Elsevier") consists of your license details and the terms and conditions provided by Elsevier and Copyright Clearance Center.

Your confirmation email will contain your order number for future reference.

[printable details](#)

License Number 4422630595079
License date Sep 05, 2018
Licensed Content Elsevier
Publisher
Licensed Content Biophysical Journal
Publication

Licensed Content Title Viscoelastic Properties of Isolated Collagen Fibrils
Licensed Content Author Zhilei Liu Shen, Harold Kahn, Roberto Ballarini, Steven J. Eppell
Licensed Content Date Jun 22, 2011
Licensed Content Volume 100
Licensed Content Issue 12
Licensed Content Pages 8
Type of Use reuse in a thesis/dissertation
Portion figures/tables/illustrations
Number of figures/tables/illustrations 1
Format both print and electronic
Are you the author of this Elsevier article? No
Will you be translating? No
Original figure numbers Figure 1.
Title of your thesis/dissertation 'STRUCTURAL CHANGES IN STRETCHED COLLAGEN FIBRILS AS A FUNCTION OF RELAXATION TIMES'
Expected completion date Sep 2018
Estimated size (number of pages) 80
Requestor Location Dalhousie University
6299 South Street



Confirmation Number: 11745980

Order Date: 09/05/2018

Customer Information

Customer: S M Asif Iqbal
Account Number: 3001331337
Organization: Dalhousie University
Email: S.Iqbal@Dal.ca
Phone: +1 (902) 414-9173
Payment Method: Invoice


This is not an invoice

Order Details

Organic & biomolecularchemistry

Billing Status:
N/A

Order detail ID: 71530957
ISSN: 1477-0539
Publication Type: e-Journal
Volume:
Issue:
Start page:
Publisher: ROYAL SOCIETY OF CHEMISTRY
Author/Editor: Royal Society of Chemistry (Great Britain)

Permission Status:  **Granted**
Permission type: Republish or display content
Type of use: Thesis/Dissertation
Order License Id: 4422640607890

Requestor type	Academic institution
Format	Print, Electronic
Portion	image/photo
Number of images/photos requested	1
The requesting person/organization	S M Asif Iqbal
Title or numeric reference of the portion(s)	Fig. 1
Title of the article or chapter the portion is from	Synthesis and biological applications of collagen-model triple-helical peptides
Editor of portion(s)	Royal Society of Chemistry
Author of portion(s)	Gregg B. Fields
Volume of serial or monograph	Volume 8
Page range of portion	1238
Publication date of portion	20th January 2010
Rights for	Main product
Duration of use	Life of current edition
Creation of copies for the disabled	no
With minor editing privileges	no



RightsLink®

[Home](#)
[Account Info](#)
[Help](#)


Title: Viscoelastic behavior of discrete human collagen fibrils

Author: René B. Svensson, Tue Hassenkam, Philip Hansen, S. Peter Magnusson

Publication: Journal of the Mechanical Behavior of Biomedical Materials

Publisher: Elsevier

Date: January 2010

Logged in as:
S M Asif Iqbal
Dalhousie University
Account #:
3001331337

[LOGOUT](#)

Copyright © 2009 Elsevier Ltd. All rights reserved.

Review Order

Please review the order details and the associated [terms and conditions](#).

No royalties will be charged for this reuse request although you are required to obtain a license and comply with the license terms and conditions. To obtain the license, click the Accept button below.

Licensed Content Publisher	Elsevier
Licensed Content Publication	Journal of the Mechanical Behavior of Biomedical Materials
Licensed Content Title	Viscoelastic behavior of discrete human collagen fibrils
Licensed Content Author	René B. Svensson, Tue Hassenkam, Philip Hansen, S. Peter Magnusson
Licensed Content Date	January 2010
Licensed Content Volume	3
Licensed Content Issue	1
Licensed Content Pages	4
Type of Use	reuse in a thesis/dissertation
Portion	figures/tables/illustrations
Number of figures/tables/illustrations	1
Format	both print and electronic
Are you the author of this Elsevier article?	No
Will you be translating?	No
Original figure numbers	Fig. 1
Title of your thesis/dissertation	'STRUCTURAL CHANGES IN STRETCHED COLLAGEN FIBRILS AS A FUNCTION OF RELAXATION TIMES'
Expected completion date	Sep 2018
Estimated size (number of pages)	80
Requestor Location	Dalhousie University 6299 South Street Halifax, NS B3H 4R2 Canada Attn: Physics
Publisher Tax ID	GB 494 6272 12
Total	0.00 USD

[Edit Order Details](#)

<https://s100.copyright.com/AppDispatchServlet>



RightsLink®

[Home](#)
[Account Info](#)
[Help](#)


Title: Viscoelastic Properties of Isolated Collagen Fibrils

Author: Zhilei Liu Shen, Harold Kahn, Roberto Ballarini, Steven J. Eppell

Publication: Biophysical Journal

Publisher: Elsevier

Date: 22 June 2011

Logged in as:
S M Asif Iqbal
Dalhousie University
Account #:
3001331337

[LOGOUT](#)

Copyright © 2011 Biophysical Society. Published by Elsevier Inc. All rights reserved.

Review Order

Please review the order details and the associated [terms and conditions](#).

No royalties will be charged for this reuse request although you are required to obtain a license and comply with the license terms and conditions. To obtain the license, click the Accept button below.

Licensed Content Publisher Elsevier

Licensed Content Publication Biophysical Journal

Licensed Content Title Viscoelastic Properties of Isolated Collagen Fibrils

Licensed Content Author Zhilei Liu Shen, Harold Kahn, Roberto Ballarini, Steven J. Eppell

Licensed Content Date 22 June 2011

Licensed Content Volume 100

Licensed Content Issue 12

Licensed Content Pages 8

Type of Use reuse in a thesis/dissertation

Portion figures/tables/illustrations

Number of figures/tables/illustrations 1

Format both print and electronic

Are you the author of this Elsevier article? No

Will you be translating? No

Original figure numbers Figure 1

Title of your thesis/dissertation 'STRUCTURAL CHANGES IN STRETCHED COLLAGEN FIBRILS AS A FUNCTION OF RELAXATION TIMES'

Expected completion date Sep 2018

Estimated size (number of pages) 80

Requestor Location Dalhousie University
6299 South Street

Halifax, NS B3H 4R2
Canada
Attn: Physics

Publisher Tax ID GB 494 6272 12

Total 0.00 CAD